aerospace

MDPI

Article

Disturbance Observer-Based Backstepping Terminal Sliding Mode Aeroelastic Control of Airfoils

Shiqian Liu [1,*], Congjie Yang [1], Qian Zhang [1] and James F. Whidborne [2]

[1] School of Aeronautics and Astronautics, Shanghai Jiao Tong University, Shanghai 200240, China; a15167773666@sjtu.edu.cn (C.Y.); zhang_qian@sjtu.edu.cn (Q.Z.)
[2] School of Aerospace, Transport and Manufacturing, Cranfield University, Cranfield MK43 0AL, UK; j.f.whidborne@cranfield.ac.uk
* Correspondence: liushiqian@sjtu.edu.cn

Abstract: This paper studies aeroelastic control for a two-dimensional airfoil–flap system with unknown gust disturbances and model uncertainties. Open loop limit cycle oscillation (LCO) happens at the post-flutter speed. The structural stiffness and quasi-steady and unsteady aerodynamic loads of the aeroelastic system are represented by nonlinear models. To robustly suppress aeroelastic vibration within a finite time, a backstepping terminal sliding-mode control (BTSMC) is proposed. In addition, a learning rate (LR) is incorporated into the BTSMC to adjust how fast the aeroelastic response converges to zero. In order to overcome the fact that the BTSMC design is dependent on prior knowledge, a nonlinear disturbance observer (DO) is designed to estimate the variable observable disturbances. The closed-loop aeroelastic control system has proven to be globally asymptotically stable and converges within a finite time using Lyapunov theory. Simulation results of an aeroelastic two-dimensional airfoil with both trailing-edge (TE) and leading-edge (LE) control surfaces show that the proposed DO-BTSMC is effective for flutter suppression, even when subjected to gusts and parameter uncertainties.

Keywords: aeroelastic two-dimensional airfoil; flutter suppression; backstepping control; fast nonsingular terminal sliding-mode control; nonlinear disturbance observer

check for updates

Citation: Liu, S.; Yang, C.; Zhang, Q.; Whidborne, J.F. Disturbance Observer-Based Backstepping Terminal Sliding Mode Aeroelastic Control of Airfoils. *Aerospace* **2024**, *11*, 882. https://doi.org/10.3390/aerospace11110882

Academic Editors: Nadjim Horri and Toufik Souanef

Received: 10 September 2024
Revised: 13 October 2024
Accepted: 14 October 2024
Published: 25 October 2024

Copyright: © 2024 by the authors. Licensee MDPI, Basel, Switzerland. This article is an open access article distributed under the terms and conditions of the Creative Commons Attribution (CC BY) license (https://creativecommons.org/licenses/by/4.0/).

1. Introduction

Nonlinear aeroelastic phenomena, such as limit cycle oscillation [1] and free play flutter [2], not only threaten the aircraft structures but can even result in loss of control. This challenge attracts many researchers to develop aeroelastic control for flutter suppression and avoidance of LCO [3]. Passive flutter control has usually been widely used for wing flutter suppression in practical engineering, including mass balance, local stiffness enhancement, etc.; however, this method requires extra mass and makes the airplane heavier [4]. Therefore, active flutter control has been proposed, and the objectives are to suppress flutter and increase the flutter speed.

Modern control theory is often proposed to suppress wing flutter. For example, Ouyang et al. studied the influence of flap camber on the wing flutter bounds and proposed a linear quadratic Gaussian (LQG)-based control to actively suppress the aeroelastic response by the flap deflection. They found that the wing flutter speed and frequency are affected by the order of the morphing flap camber geometry model [5]. Na et al. proposed an LQG control method with a sliding mode control (SMC) observer to actively control composite thin-walled beam structures in compressible flow; the dynamic aeroelastic responses to sharp-edged gusts, blast loads, and sonic booms were investigated [6].

Aeroelastic systems are subjected to nonlinearities and other complex effects, resulting from freeplay, time delays, and cubic nonlinearities. Neil et al. explored the effects of structural nonlinearity by analyzing and experimenting with a rigid wing supported by a nonlinear spring [7]. Lee et al. examined the effect of a cubic structural restoring force

on the flutter of a two-dimensional airfoil placed in incompressible flow. Their results demonstrated that the divergence flutter boundary depends on the initial conditions for a soft spring, and it remains independent of them for a hard spring [8]. To stabilize a nonlinear aeroelastic system, Singh et al. proposed an adaptive backstepping output feedback control scheme and trajectory control of the pitch angle [9].

To address the model uncertainties in aeroelastic systems, Lin et al. suggested a decoupled fuzzy sliding mode control (DFSMC), and the DFSMC system was designed to control the plunge and pitch motions simultaneously [10]. Chen et al. proposed a terminal SMC (TSMC) for aeroelastic systems; the LCO suffered in an aeroelastic system was removed by the TSMC [11]. Mukhopadhyay introduced a historical perspective on the analysis and control of aeroelasticity over the century and showed some experiments of aeroelastic control for different aircraft [3].

Bouma et al. investigated structural and aerodynamic nonlinear effects for three-degree-of-freedom (DOF) aeroelastic systems; stall effects were introduced using quasi-steady and unsteady aerodynamic representations [12]. Vishal et al. studied the synchronization characteristics of a pitch–plunge aeroelastic system, possessing discontinuous nonlinearities in both structural and aerodynamic fronts. Meanwhile, a multi-physics fluid–structure interaction problem possessing coupled non-smooth nonlinearities can be alleviated by the use of synchronization theory [13]. Livne provided a survey on state-of-the-art aircraft active flutter suppression (AFS) through AFS wind tunnel testing and flight-test programs [14].

Flutter suppression theory has also been developed by researchers. Considering the delayed control problem, a single time delay was determined according to both the critical stability condition and the stability margins, and Zou et al. proposed a simple scheme consisting of a delayed proportional–differential (PD) controller to robustly suppress the body-freedom flutter (BBF) of a flying-wing drone [15]. Trapani and Guo proposed a rudderless aeroelastic fin for a flexible blended-wing-body UAV to improve the divergence and flutter margin [16]. Although these methods are useful for linear time-invariant systems, they cannot guarantee the closed-loop performances of nonlinear and time-varying aeroelastic systems.

To cope with structural nonlinearities and unsteady flow, Zhang and Behal proposed a continuous robust controller for aeroelastic vibration control of a two-dimensional airfoil [17]. Lee and Singh proposed an L_1 adaptive control for an aeroelastic system with unsteady aerodynamics and gust loads [18]. For nonlinear aeroelastic systems, Platanitis and Strganac proposed feedback linearization combined with a model reference that can adaptively control and suppress the LCO of a typical wing section with both leading-edge and trailing-edge control surfaces [19]. Prime proposed a linear-parameter-varying model for the three-DOF Nonlinear Aeroelastic Test Apparatus (NATA) model and developed an H_2 robust control via linear matrix inequalities [20]. Li et al. proposed a state-dependent Riccati equation-based method to control an airfoil section with control surface nonlinearities, but it depended on an accurate model [21]. To reduce dependence on the model, Tang et al. proposed neural-network-based active flutter suppression under control input constraints [22], but neural networks require extensive calculations. Recently, Gao introduced sliding-mode control into an aeroelastic system and presented a finite-time fault-tolerant control for wing flutter suppression [23]. Chen et al. proposed a model-free deep reinforcement learning algorithm for active flutter suppression through aeroelastic wind tunnel testing; thus, the jet flow intensity can be intelligently selected according to the real-time state of the flexible wing [24].

Because aircraft fly within varying environments, the influence of model uncertainties and external disturbances on aeroelastic systems have also been considered by researcher. Pettit briefly described aerodynamic and structural uncertainties and applications of uncertainty with design optimization [25]. For nonlinear perturbations, Hao et al. analyzed stochastic nonlinear flutter behaviors of a three-DOF wing model using the stochastic

p-bifurcation analysis method [26]. Lee and Singh proposed a robust higher-order super-twisting control to control an aeroelastic system with unsteady aerodynamics [27].

To estimate unknown parameters, Prabhu and Srinivas proposed an intelligent observer and then robust control of a three-DOF aeroelastic model [28], but the neural network-based observer has a heavy computational load. To improve the convergence speed of the aeroelastic system, Chen et al. proposed a TSMC to reach the target within a finite time frame [11], while Yuan et al. proposed a sliding-mode observer control for a two-dimensional aeroelastic system with gusts [29]. Xu et al. also applied backstepping sliding-mode control (BSMC) design to suppress the LCO in the presence of uncertainties and external disturbances [30].

All these methods can suppress or attenuate external disturbances and achieve the desired robust performance; however, an alternative approach is available, the so-called disturbance-observer-based control (DOBC). DOBC lumps all internal uncertainties and external disturbances acting on the aeroelastic system into a single term and then identifies them using the DO. The DO can provide fast, excellent control performances and smooth control actions without requiring large feedback gains [31]. Liu and Whidborne have proposed a nonlinear disturbance observer to deal with bounded unknown disturbances [32], but this observer is less effective with variable disturbances, and the output tracking responses of this DO-BSMC are not guaranteed to converge within a finite time.

Motivated by the work of Xu [30] and Chen [31], this paper considers trajectory tracking control for a two-dimensional airfoil–flap aeroelastic system. The main contributions of this research are as follows:

Considering quasi-steady and unsteady aerodynamic loads, nonlinear dynamic models are set up for an aeroelastic two-dimensional airfoil with both trailing-edge and leading-edge control surfaces.

To suppress flutter, a backstepping terminal sliding-mode control is proposed for the two-dimensional airfoil–flap aeroelastic system. The benefits of this approach include the TSMC merits of high robustness, fast transient response, and finite-time convergence, as well as backstepping control in terms of globally asymptotic stability.

To overcome the limitation of the BTSMC being dependent on prior knowledge, a nonlinear disturbance observer is designed for coping with model uncertainties and variable external bounded gust disturbances, which is different from the backstepping SMC for flutter suppression [30].

To adjust the speed of the aeroelastic response converging to zero, a learning rate is incorporated into the BTSMC design.

Simulation results show that the proposed DO-BTSMC method is effective and has advantages in LCO suppression and flutter control for a two-dimensional wing with LE and TE control surfaces.

This paper is organized as follows: Section 2 establishes the nonlinear aeroelastic dynamics model of the two-dimensional airfoil–flap system. Section 3 proposes a DO-BTSMC design, and stability is analyzed for the closed-loop control system. Simulations and analysis are in Section 4. Some conclusions are given in Section 5.

2. Aeroelastic System Dynamic Model

The studied model is a two-DOF pitch–plunge wing section with both LE and TE control surfaces and is shown in Figure 1. Both control surfaces are used as control inputs. Also shown are the wing physical parameters; a is the non-dimensional distance from the wing section mid-chord to the elastic axis position, b denotes the semi-chord length, and c is the full chord length.

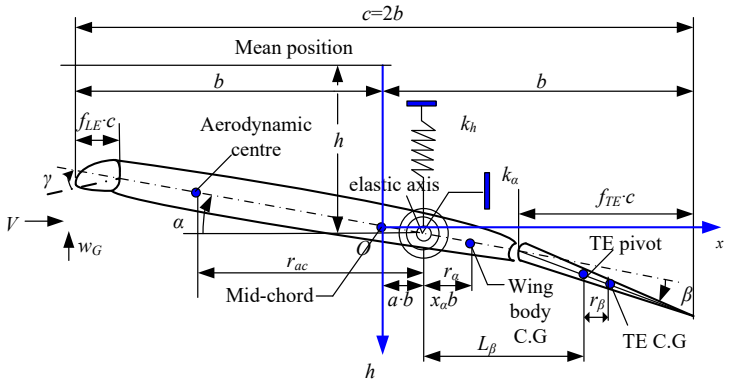

Figure 1. Model of the two-dimensional flexible wing.

The aeroelastic governing models are established as follows [19]:

$$\begin{bmatrix} m_T & m_w x_\alpha b \\ m_w x_\alpha b & I_\alpha \end{bmatrix} \begin{bmatrix} \ddot{h} \\ \ddot{\alpha} \end{bmatrix} + \begin{bmatrix} c_h & 0 \\ 0 & c_\alpha \end{bmatrix} \begin{bmatrix} \dot{h} \\ \dot{\alpha} \end{bmatrix} + \begin{bmatrix} k_h & 0 \\ 0 & k_\alpha(\alpha) \end{bmatrix} \begin{bmatrix} h \\ \alpha \end{bmatrix} = \begin{bmatrix} -L \\ M \end{bmatrix}, \tag{1}$$

where

$$L = \rho V^2 b s_p C_{L\alpha} \left(\alpha + \frac{\dot{h}}{V} + \left(\frac{1}{2} - a \right) b \frac{\dot{\alpha}}{V} \right) + \rho V^2 b s_p C_{L\beta} \beta + \rho V^2 b s_p C_{L\gamma} \gamma, \tag{2}$$

$$M = \rho V^2 b^2 s_p C_{m\alpha,eff} \left(\alpha + \frac{\dot{h}}{V} + \left(\frac{1}{2} - a \right) b \frac{\dot{\alpha}}{V} \right) + \rho V^2 b^2 s_p C_{m\beta,eff} \beta + \rho V^2 b^2 s_p C_{m\gamma,eff} \gamma, \tag{3}$$

and $C_{m\alpha,eff}$, $C_{m\beta,eff}$, and $C_{m\gamma,eff}$ are the effective dynamic and control moment derivatives due to the angle of attack and trailing- and leading-edge control surface deflection, respectively, about the elastic axis and are defined as follows:

$$C_{m\alpha,eff} = (0.5+a) C_{L\alpha} + 2C_{m\alpha}, C_{m\beta,eff} = (0.5+a) C_{L\beta} + 2C_{m\beta},$$

$$C_{m\gamma,eff} = (0.5+a) C_{L\gamma} + 2C_{m\gamma}, \tag{4}$$

where m_T denotes the total mass of the pitch–plunge system; c_α and c_h denote the damping of the pitch and plunge, respectively; k_α and k_h denote pitch and plunge stiffness, respectively; s_p is the wing section span; I_α denotes the total pitch moment of inertia about the elastic axis; ρ denotes the air density; h is the plunge displacement; V is the freestream velocity; α is the angle of attack (AOA); β and γ denote the trailing- and leading-edge control surface deflections, respectively; C_L, $C_{L\alpha}$, $C_{L\beta}$, $C_{L\gamma}$ denote the wing section lift coefficients; and C_m, $C_{m\alpha}$, $C_{m\beta}$, $C_{m\gamma}$ denote the wing section pitch moment coefficients at the quarter-chord.

The state variable vector is denoted as

$$\boldsymbol{x}_1 = \begin{bmatrix} h & \alpha \end{bmatrix}^T, \boldsymbol{x}_2 = \dot{\boldsymbol{x}}_1 = \begin{bmatrix} \dot{h} & \dot{\alpha} \end{bmatrix}^T, \boldsymbol{x} = \begin{bmatrix} \boldsymbol{x}_1^T & \boldsymbol{x}_2^T \end{bmatrix}^T, \tag{5}$$

$$\dot{\boldsymbol{x}}_2(t) = \boldsymbol{f}_2(\boldsymbol{x}) + \boldsymbol{g}_2(\boldsymbol{x}) U(t), \tag{6}$$

$$\boldsymbol{f}_2(\boldsymbol{x}) = \begin{bmatrix} -k_1 & -k_2 V^2 + p(x_2) \\ -k_3 & -k_4 V^2 + q(x_2) \end{bmatrix} \boldsymbol{x}_1 + \begin{bmatrix} -c_1 & -c_2 \\ -c_3 & -c_4 \end{bmatrix} \boldsymbol{x}_2, U = \begin{bmatrix} \beta \\ \gamma \end{bmatrix}, \boldsymbol{g}_2(\boldsymbol{x}) = \begin{bmatrix} g_{2,11} & g_{2,12} \\ g_{2,21} & g_{2,22} \end{bmatrix},$$

$$\Xi = m_T I_a - (m_W x_\alpha b)^2, k_1 = I_a k_h / \Xi, k_3 = -m_W x_\alpha b k_h / \Xi,$$

$$k_2 = \left(I_a \rho s_p b C_{L\alpha} + m_W x_\alpha \rho s_p b^3 C_{m\alpha} \right) / \Xi, k_4 = -\left(m_W x_\alpha \rho s_p b^2 C_{L\alpha} + m_T \rho s_p b^2 C_{m\alpha,eff} \right) / \Xi,$$

$$c_1 = \left(I_\alpha \left(c_h + \rho V s_p b C_{L\alpha} \right) + m_W x_\alpha \rho V s_p b^3 C_{m\alpha,eff} \right) / \Xi,$$

$$
\begin{aligned}
c_2 &= \left(I_\alpha \rho V s_p b^2 C_{L\alpha}(0.5-a) - m_W x_\alpha b c_\alpha + m_W x_\alpha \rho V s_p b^4 C_{m\alpha,eff}(0.5-a)\right)/\Xi,\\
c_3 &= \left(-m_W x_\alpha b\left(c_h + \rho V b s_p C_{L\alpha}\right) - m_T \rho V s_p b^2 C_{m\alpha,eff}\right)/\Xi,\\
c_4 &= \left[m_T\left(c_\alpha - \rho V s_p b^3 C_{m\alpha,eff}(0.5-a)\right) - m_W x_\alpha \rho V s_p b^3 C_{L\alpha}(0.5-a)\right]/\Xi,\\
g_{2,11} &= \left(-I_\alpha \rho b s_p C_{L\beta} - m_W x_\alpha \rho s_p b^3 C_{m\beta,eff}\right)V^2/\Xi,\\
g_{2,21} &= \left(-I_\alpha \rho b s_p C_{L\gamma} - m_W x_\alpha \rho s_p b^3 C_{m\gamma,eff}\right)V^2/\Xi,\\
g_{2,21} &= \left(m_W x_\alpha \rho s_p b^2 C_{L\beta} + m_T \rho s_p b^2 C_{m\beta,eff}\right)V^2/\Xi,\\
g_{2,22} &= \left(m_W x_\alpha \rho s_p b^2 C_{L\gamma} + m_T \rho s_p b^2 C_{m\gamma,eff}\right)V^2/\Xi,
\end{aligned} \tag{7}
$$

and the uncertain functions of plunge and AOA motions are

$$
q(x_2) = m_T k_\alpha/\Xi,\ p(x_2) = -m_W x_a b k_a/\Xi. \tag{8}
$$

The servo motor dynamics for the TE and LE can be modeled as second-order systems of the form

$$
\begin{cases} I_\beta \ddot{\beta} + c_{\beta s}\dot{\beta} + k_{\beta s}\beta = k_{\beta s}\beta_c \\ I_\gamma \ddot{\gamma} + c_{\gamma s}\dot{\gamma} + k_{\gamma s}\gamma = k_{\gamma s}\gamma_c \end{cases}, \tag{9}
$$

where $c_{\beta s}$ and $c_{\gamma s}$ are the dampings of the TE and LE, respectively; $k_{\beta s}$ and $k_{\gamma s}$ are the stiffness of the TE and LE, respectively; and β_c and γ_c denote the desired positions of the servo motors for the TE and LE, respectively. The terms m_α and $I_{\alpha 0}$ denote the rotational wing body mass and inertia, respectively; $I_\alpha = I_{\alpha 0} + m_\alpha x_\alpha^2 b^2$, $I_\beta = I_{\beta 0} + m_\beta r_\beta^2$, and $I_\gamma = I_{\gamma 0} + m_\gamma r_\gamma^2$ are the moments of inertia of the TE and LE about their respective pivots; m_β and m_γ are the rotational TE and LE sections of mass, respectively; and $I_{\beta 0}$ and $I_{\gamma 0}$ are the rotational TE and LE sections of inertia, respectively. Let $\overline{m} = m_h + m_\alpha + m_\beta + m_\gamma$ hold, where m_h denotes the translational body mass.

When the aerodynamic performance of the airfoil is unsteady, the equations of motion for the entire system can be set up using Lagrangian energy theory,

$$
\frac{d}{dt}\begin{bmatrix} \partial\mathcal{L}/\partial h \\ \partial\mathcal{L}/\partial\alpha \\ \partial\mathcal{L}/\partial\beta \\ \partial\mathcal{L}/\partial\gamma \end{bmatrix} - \begin{bmatrix} \partial\mathcal{L}/\partial h \\ \partial\mathcal{L}/\partial\alpha \\ \partial\mathcal{L}/\partial\beta \\ \partial\mathcal{L}/\partial\gamma \end{bmatrix} = -\begin{bmatrix} 0 \\ 0 \\ k_{\beta s}\beta \\ k_{\gamma s}\gamma \end{bmatrix} - \begin{bmatrix} c_h\dot{h} \\ c_\alpha\dot{\alpha} \\ c_{\beta s}\dot{\beta} \\ c_{\gamma s}\dot{\gamma} \end{bmatrix} + \begin{bmatrix} -L \\ M_\alpha \\ M_\beta \\ M_\gamma \end{bmatrix} + \begin{bmatrix} 0 \\ 0 \\ k_{\beta s}\beta_c \\ k_{\gamma s}\gamma_c \end{bmatrix}, \tag{10}
$$

where $\mathcal{L}$ denotes a Lagrangian function. The expanded form of Equation (10) is

$$
\begin{bmatrix} \overline{m} & \xi_1 & m_\beta r_\beta & m_\gamma r_\gamma \\ * & \xi_2 & I_\beta + x_\beta m_\beta r_\beta & I_\gamma + x_\gamma m_\gamma r_\gamma \\ * & * & I_\beta & 0 \\ * & * & 0 & I_\gamma \end{bmatrix}\begin{bmatrix} \ddot{h} \\ \ddot{\alpha} \\ \ddot{\beta} \\ \ddot{\gamma} \end{bmatrix} + \begin{bmatrix} k_h h + c_h\dot{h} + \xi_3 \\ k_\alpha\alpha + c_\alpha\dot{\alpha} + \xi_4 \\ k_{\beta s}\beta + c_{\beta s}\dot{\beta} + \alpha^2 m_\beta r_\beta x_\beta \sin\beta \\ k_{\gamma s}\gamma + c_{\gamma s}\dot{\gamma} + \alpha^2 m_\gamma r_\gamma x_\gamma \sin\gamma \end{bmatrix} = \begin{bmatrix} -L \\ M_\alpha \\ M_\beta \\ M_\gamma \end{bmatrix} + \begin{bmatrix} 0 \\ 0 \\ k_{\beta s}\beta_c \\ k_{\gamma s}\gamma_c \end{bmatrix} \tag{11}
$$

where * denotes an asymmetric matrix element, and

$$
\begin{aligned}
\xi_1 &= (m_\alpha r_\alpha + m_\beta r_\beta + m_\gamma r_\gamma)\cos\alpha + m_\beta r_\beta \cos(\alpha+\beta) + m_\gamma r_\gamma \cos(\alpha+\gamma),\\
\xi_2 &= I_\alpha + I_\beta + I_\gamma + m_\beta x_\beta^2 + m_\gamma x_\gamma^2 + 2x_\beta m_\beta r_\beta \cos\beta + 2x_\gamma m_\gamma r_\gamma \cos\gamma,\\
\xi_3 &= -(\alpha+\beta)^2 m_\beta r_\beta \sin(\alpha+\beta) - (\alpha+\gamma)^2 m_\gamma r_\gamma \sin(\alpha+\gamma) - \alpha^2 \sin\alpha(m_\alpha r_\alpha + m_\beta x_\beta + m_\gamma x_\gamma),\\
\xi_4 &= -\beta(2\alpha+\beta) m_\beta r_\beta x_\beta \sin(\beta) - \gamma(2\alpha+\gamma) m_\gamma r_\gamma x_\gamma \sin(\gamma).
\end{aligned} \tag{12}
$$

The aerodynamic force and moment in Equation (10) can be calculated by Theodorsen's method [33,34]:

$$\begin{aligned} L = {} & \pi\rho b^2 s_p\left(\ddot{h} + V\dot{\alpha} - ba\ddot{\alpha} - (V/\pi)T_4\dot{\beta} - (b/\pi)T_1\ddot{\beta} + (V/\pi)T_4\dot{\gamma} - (b/\pi)T_1\ddot{\gamma}\right) \\ & +2\pi\rho V b s_p C(k)\left(V\alpha + \dot{h} + b(0.5-a)\dot{\alpha} + (V/\pi)T_{10}\beta + (b/2\pi)T_{11}\dot{\beta} + (V/\pi)T_{10}\gamma + (b/2\pi)T_{11}\dot{\gamma}\right), \end{aligned} \tag{13}$$

$$\begin{aligned} M_\alpha = \pi\rho b^2 s_p \quad & \left(ba\ddot{h} - Vb(0.5-a)\dot{\alpha} - b^2(1/8+a)\ddot{\alpha} - (V^2/\pi)T_{15}(\beta+\gamma) - (Vb/\pi)T_{16}(\dot{\beta}+\dot{\gamma}) - 2(b^2/\pi)T_{13}(\ddot{\beta}+\ddot{\gamma})\right) \\ & +2\pi\rho V b^2 s_p(a+0.5)C(k)\left(V\alpha + \dot{h} + b(0.5-a)\dot{\alpha} + (V/\pi)T_{10}(\beta+\gamma) + (b/2\pi)T_{11}(\dot{\beta}+\dot{\gamma})\right), \end{aligned} \tag{14}$$

$$\begin{aligned} M_\beta = {} & -\rho b^2 s_p\left((-2T_9 - T_1 + T_4(a-0.5))Vb\dot{\alpha} + 2T_{13}b^2\ddot{\alpha} + (1/\pi)V^2(\beta+\gamma)(T_5 - T_4T_{10})\right. \\ & \left.-(1/2\pi)Vb(\dot{\beta}+\dot{\gamma})T_4T_{11} - (1/\pi)T_3b(\ddot{\beta}+\ddot{\gamma}) - T_1b\ddot{h}\right) \\ & -\rho V b^2 s_p T_{12}C(k)\left(V\alpha + \dot{h} + b(0.5-a)\dot{\alpha} + (1/\pi)T_{10}V(\beta+\gamma) + b(1/2\pi)T_{11}(\dot{\beta}+\dot{\gamma})\right), \end{aligned} \tag{15}$$

where T_i (i = 1, 2, . . ., 14) are the Theodorsen constants; see Appendix B [35]. M_γ is derived from these by Throdorsen [33–35].

The aerodynamic force and moments in Equations (13)–(15) are dependent on the Theodorsen function $C(k)$, where k is the non-dimensional reduced frequency of harmonic oscillation; $C(k)$ can be approximated by Jones's method,

$$C(s) = 1 - \frac{0.165s}{s + 0.0455V/b} - \frac{0.335s}{s + 0.3V/b} = \frac{1}{2} + \frac{c_1 V/b}{s + c_3 V/b} + \frac{c_2 V/b}{s + c_4 V/b}, \tag{16}$$

where c_1 = 0.0075, c_2 = 0.10055, c_3 = 0.0455, and c_4 = 0.3. $C(s)$ can be presented as a state-space model as follows:

$$\begin{cases} \begin{bmatrix} \dot{x}_{a1} \\ \dot{x}_{a2} \end{bmatrix} = \frac{V}{b}\begin{bmatrix} -c_3 & 0 \\ 0 & -c_4 \end{bmatrix}\begin{bmatrix} x_{a1} \\ x_{a2} \end{bmatrix} + \begin{bmatrix} 1 \\ 1 \end{bmatrix} r \\ y_a = \frac{V}{b}\begin{pmatrix} c_1 & c_2 \end{pmatrix}\begin{bmatrix} x_{a1} \\ x_{a2} \end{bmatrix} + 0.5r \end{cases}, \tag{17}$$

where

$$r = V\alpha + \dot{h} + b(0.5-a)\dot{\alpha} + (V/\pi)T_{10}\beta + b(1/2\pi)\dot{\beta}. \tag{18}$$

The aerodynamic force and moments can be described as the sum of non-circulatory and circulatory loads,

$$F_{ac} = F_{nc} + F_c, \tag{19}$$

where F_{nc} and F_c are the non-circulatory and circulatory loads respectively. We denote $\bar{x}_1 = \begin{bmatrix} h & \alpha & \beta & \gamma \end{bmatrix}^T$ and $x_a = [x_{a1}, x_{a2}]^T$, and then we obtain

$$F_{nc} = -M_{nc}\ddot{\bar{x}}_1 - VC_{nc}\dot{\bar{x}}_1 - V^2K_{nc}\bar{x}_1, \tag{20}$$

$$F_c = -\rho V b s_p R_c\left(\frac{V}{b}\begin{pmatrix} c_1 & c_2 \end{pmatrix}x_a + 0.5\left(S_1\dot{\bar{x}}_1 + VS_2\bar{x}_1\right)\right), \tag{21}$$

where x_α is the non-dimensional distance from the elastic axis to the center of mass, and $x_\alpha = r_{cg}/b$, where r_{cg} is the distance from the elastic axis to the center of mass, and

$$
\begin{aligned}
&M_{nc} = \rho b^2 s_p \begin{bmatrix} \pi & -\pi b a & -bT_1 & -bT_1 \\ -\pi b\bar{a} & \pi b^2(1/8+a^2) & 2b^2T_{13} & -b^2T_{13d} \\ -bT_1 & 2b^2T_{13} & -T_3b^2/\pi & 0 \\ -bT_1 & 2b^2T_{13d} & 0 & -T_3b^2/\pi \end{bmatrix}, \\
&K_{nc} = \rho b^2 s_p \begin{bmatrix} 0 & 0 & 0 & 0 \\ 0 & 0 & T_{15} & T_{15} \\ 0 & 0 & T_{18}/\pi & 0 \\ 0 & 0 & 0 & T_{18}/\pi \end{bmatrix}, \\
&R_c = \begin{bmatrix} 2\pi & -2\pi b(0.5+a) & T_{12} & T_{12} \end{bmatrix}^T, S_1 = \begin{bmatrix} 1 & b(0.5-a) & bT_{11}/(2\pi) & bT_{11}/(2\pi) \end{bmatrix}, \\
&S_2 = \begin{bmatrix} 0 & 1 & \mathrm{T}_{10}/\pi & \mathrm{T}_{10}/\pi \end{bmatrix},
\end{aligned} \tag{22}
$$

where T_{13} and T_{13d} are the Theodorsen constants for the TE and LE. respectively. Substituting Equations (17) and (13)–(15) into Equation (11) then yields

$$
(M_s + M_{nc})\ddot{\bar{x}}_1 + (C_s + VC_{nc} + VC_c)\dot{\bar{x}}_1 + \left(K_s + V^2K_{nc} + V^2K_c\right)\bar{x}_1 = -V^2E_cx_a + G_su_c \tag{23}
$$

where

$$
\begin{aligned}
&C_{nc} = \rho b^2 s_p \begin{bmatrix} 0 & \pi & -T_4 & T_4 \\ 0 & \pi b(0.5-\bar{a}) & bT_{16} & bT_{16} \\ 0 & bT_{17} & bT_{19}/\pi & 0 \\ 0 & bT_{17} & 0 & bT_{19}/\pi \end{bmatrix}, C_s = \begin{bmatrix} c_h & 0 & 0 & 0 \\ 0 & c_\alpha & 0 & 0 \\ 0 & 0 & c_{\beta\mathrm{s}} & 0 \\ 0 & 0 & 0 & c_{\gamma\mathrm{s}} \end{bmatrix}, \\
&K_s = \begin{bmatrix} k_h & 0 & 0 & 0 \\ 0 & k_\alpha & 0 & 0 \\ 0 & 0 & k_{\beta s} & 0 \\ 0 & 0 & 0 & k_{\gamma s} \end{bmatrix}, G_s = \begin{bmatrix} 0 & 0 \\ 0 & 0 \\ k_{\beta s} & 0 \\ 0 & k_{\gamma s} \end{bmatrix}, M_s = \begin{bmatrix} \overline{m} & \xi_1 & m_\beta r_\beta & m_\gamma r_\gamma \\ * & \xi_2 & I_\beta + x_\beta m_\beta r_\beta & I_\gamma + x_\gamma m_\gamma r_\gamma \\ * & * & I_\beta & 0 \\ * & * & 0 & I_\gamma \end{bmatrix} \\
&C_c = \tfrac{1}{2}\rho b s_p R_c S_1, K_c = \tfrac{1}{2}\rho b s_p R_c S_2, E_c = \rho s_p R_c \begin{bmatrix} c_1 & c_2 \end{bmatrix}, u_c = [\beta_c, \gamma_c]^{\mathrm{T}},
\end{aligned} \tag{24}
$$

The full state vector is denoted as $\bar{x} = \begin{bmatrix} \bar{x}_1{}^T & \dot{\bar{x}}_1{}^T & x_a^T \end{bmatrix}^T$, and the overall state-space model is

$$
\dot{\bar{x}} = \boldsymbol{A}\bar{x} + \boldsymbol{B}u, \tag{25}
$$

where the **A** and **B** matrices are as follows:

$$
\boldsymbol{A} = \begin{bmatrix} 0 & I & 0 \\ -M^{-1}K(V) & -M^{-1}C(V) & -V^2M^{-1}E_c \\ VK_a & C_a & VA_a \end{bmatrix}, \boldsymbol{B} = \begin{bmatrix} 0 \\ M^{-1}G_s \\ 0 \end{bmatrix}, \tag{26}
$$

where

$$
\begin{aligned}
&M = M_{nc} + M_s, K(V) = K_s + V^2K_{nc} + V^2K_c, C(V) = C_s + VC_{nc} + VC_c, \\
&K_a = \begin{bmatrix} 1 \\ 1 \end{bmatrix} S_2, C_a = \begin{bmatrix} 1 \\ 1 \end{bmatrix} S_1, A_a = \tfrac{1}{b}\begin{bmatrix} -c_3 & 0 \\ 0 & -c_4 \end{bmatrix}.
\end{aligned} \tag{27}
$$

Since there exists wind disturbance for the aeroelastic system, the external disturbance $\boldsymbol{D}$ is considered and added into the system of Equations (6) and (25) as

$$
\begin{cases} \dot{x}_2(t) = f_2(x) + g_2(x)U(t) + \boldsymbol{D}(t), & \text{(Quasi-steady load case)} \\ \ddot{\bar{x}}_1(t) = -M^{-1}\left(K(V)\bar{x}_1 + C(V)\dot{\bar{x}}_1 + V^2E_cx_a\right) + M^{-1}G_su + \overline{\boldsymbol{D}}(t), & \text{(Unsteady load case)} \end{cases} \tag{28}
$$

where $\boldsymbol{D} \in R^2$ and $\overline{\boldsymbol{D}}(t) \in R^4$ denote external disturbances and are bounded by $\|D\| < D_U$, where D_U is a real value meeting $D_\mathrm{U} \geq 0, \bar{f}_2(\bar{x}_1) = -M^{-1}\left(K(V)\bar{x}_1 + C(V)\dot{\bar{x}}_1 + V^2E_cx_a\right)$,

and $\overline{g}_2(\overline{x}_1) = M^{-1}G_s$. The aerodynamic loads due to the wind disturbances are defined as [36]

$$L_g = \rho V^2 b s_p C_{L\alpha} \omega_G(\tau)/V = \rho V b s_p C_{L\alpha} \omega_G(\tau), \tag{29}$$

$$M_g = (0.5 + a) b L_g, \tag{30}$$

where $\omega_G(\tau)$ denotes the disturbance velocity and τ is a dimensionless time variable defined as $\tau = Vt/b$, so $\boldsymbol{D} = \begin{bmatrix} -L_g/m_T & M_g/I_\alpha \end{bmatrix}^T$. Suppose that the above disturbance can be generated by a linear exogenous system [31],

$$\begin{cases} \dot{\varsigma}_d(t) = W_d \varsigma_d(t) \\ D(t) = V_d \varsigma_d(t) \end{cases}, \tag{31}$$

where $\varsigma_d \in R^p$, W_d, and V_d are coefficient matrices with corresponding dimensions.

Airfoil Aeroelastic Vibration Control Problem: The control objective is to suppress the aeroelastic vibrations, so the desired smooth trajectory $\boldsymbol{x}_d$ can be chosen to be zero for all time. Alternatively, the desired trajectory $\boldsymbol{x}_d$ along with the actual pitching and plunging variables is driven towards the origin.

3. DO-BTSMC Aeroelastic Control Design

This section gives an overview of the DO-BTSMC control for the two-dimensional airfoil.

3.1. Nonlinear Disturbance Observer Design

Considering unknown disturbances in the aeroelastic system (28), a nonlinear disturbance observer (NDO) is proposed to improve the tracking precision [31],

$$\begin{cases} \dot{z}_d(t) = (W_d - l(x)V_d)z_d(t) + W_d p_d(x) - l(x)(V_d p_d(x) + f_2(x) + g_2 U(t)) \\ \hat{\varsigma}_d(t) = z_d(t) + p_d(x) \\ \hat{D}(t) = V_d \hat{\varsigma}_d(t) \end{cases}, \tag{32}$$

where $\hat{D}$ is the estimated disturbance, $l\,(x)$ is the vector of observer gains to be tuned for performance, z_d is the internal state vector, and $p_d(x)$ is a nonlinear function to be designed. The NDO gain $l(x)$ is determined by

$$l(x) = \frac{\partial p_d(x)}{\partial x}, \tag{33}$$

Integrating $l(x_2)$ with respect to the aeroelastic system state x yields

$$p_d(x) = L_d Lie_f^{r-1} \hbar(x) \tag{34}$$

where L_d is a gain vector, Lie_f denotes a Lie derivative of the function $f(x)$, and r is the relative degree. We select $\hbar(x_2) = x_2$. The nonlinear disturbance estimation error is $d = \boldsymbol{D} - \hat{D}$.

It has been shown that the estimation $\hat{D}$ of the NDO approaches the disturbance $D(t)$ exponentially if the observer gain $l(x)$ is chosen such that (32) is globally exponentially stable for all $x \in R^n$ [37]. The estimation of harmonic disturbance, $\hat{D}$, yielded by the DO of Equation (32) approaches the disturbance, $\boldsymbol{D}$, and is globally exponentially stable if the following inequalities are satisfied [31]:

$$V = \frac{1}{2\gamma_d} d^T d > 0, \dot{V} < 0 \tag{35}$$

Hence, the disturbance compensator can be designed as

$$u_d(t) = -g_2^{-1} \hat{D}(t) \tag{36}$$

When the nonlinear disturbance observer is used, $\hat{D}$ will approach $\boldsymbol{D}$, so the disturbance can be attenuated through the disturbance compensator (36), and the system (28) can be transformed as follows:

$$\begin{aligned} \dot{x}_2(t) &= f_2(x_1, x_2) + g_2 U(t) + \boldsymbol{D} \\ &= f_2(x_1, x_2) + g_2(U_{BTSMC}(t) + u_d(t)) + \boldsymbol{D}(t) \\ &= f_2(x) + g_2(x) U_{BTSMC}(t) + d, \end{aligned} \tag{37}$$

The observable disturbances, such as 1-cosine winds, usually can be measured and estimated by the observer. It has been shown that the estimation $\hat{\boldsymbol{D}}(t)$ of the NDO approaches the disturbance $\boldsymbol{D}(t)$ exponentially if the error dynamics for $d(t)$ is globally exponentially stable [31]. By a similar method, the disturbances $\overline{\boldsymbol{D}}(t)$ for unsteady loads can also be estimated.

3.2. DO-BTSMC-Based Aeroelastic Control Design

To drive the aeroelastic output $\boldsymbol{x}$ to converge to the desired value vector $\boldsymbol{x_d}$, the aeroelastic controller is designed as follows:

The tracking error vector of the plunge displacement and pitch angle is defined as

$$\boldsymbol{z}_1 = \boldsymbol{x}_1 - \boldsymbol{x}_{1d}, \tag{38}$$

and its derivative is

$$\dot{\boldsymbol{z}}_1 = \dot{\boldsymbol{x}}_1 - \dot{\boldsymbol{x}}_{1d} = \boldsymbol{x}_2 - \dot{\boldsymbol{x}}_{1d} \tag{39}$$

The stabilizing function $\phi_1(x)$ is defined as the virtual speed vector of $\dot{\boldsymbol{x}}_{1d}$:

$$\phi_1(x_1) = \dot{\boldsymbol{x}}_{1d} - K_1 \boldsymbol{z}_1, \tag{40}$$

where $\dot{\boldsymbol{x}}_{1d}$ represents the reference or virtual speed vector, and $K_1 > 0$ is often chosen as a diagonal matrix to simplify the design; i.e., K_1 =diag(k_{11}, k_{12}), where k_{1i} (i = 1, 2) is a constant value.

The Lyapunov function V_1 is constucted as follows:

$$V_1 = \frac{1}{2} \boldsymbol{z}_1^T \boldsymbol{z}_1. \tag{41}$$

The speed tracking error vector for the plunge and pitch dynamics is defined as

$$\boldsymbol{z}_2 = \dot{\boldsymbol{x}}_1 - \phi_1(x_1) = \boldsymbol{x}_2 - \phi_1(x_1). \tag{42}$$

and its derivative is

$$\dot{\boldsymbol{z}}_2 = \ddot{\boldsymbol{x}}_1 - \ddot{\boldsymbol{x}}_{1d} + K_1 \dot{\boldsymbol{z}}_1. \tag{43}$$

The detailed derivation is given in the Appendix A.

Remark 1. *If there are uncertainties for the system (28), then f_2 and g_2 will include uncertain terms; the uncertain terms can be regarded as disturbances and added into D, and then the observer (32) can be used with nominal f_2 and g_2.*

Therefore, the structure of the DO-BTSMC controller for aeroelastic control is designed as shown in Figure 2, which includes the aeroelastic dynamics system of the two-dimensional airfoil, an adaptive BTSMC used for aeroelastic flutter suppression, a nonlinear DO used to estimate observable disturbances, and an adaptive disturbance estimator used to observe the unobservable disturbances. A learning rate is applied to speed up the convergence of the proposed sliding-mode control.

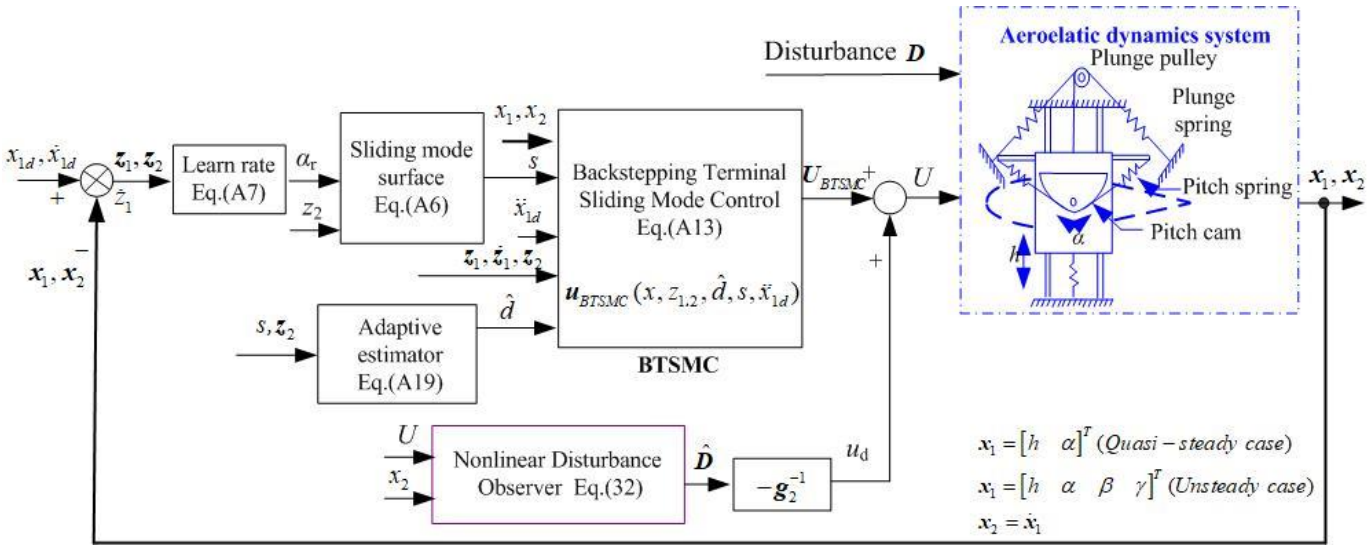

Figure 2. Block diagram of the proposed DO-BTSMC controller.

4. Discussion

The studied aeroelastic system is the NATA model, and the physical parameters of the aeroelastic system are listed in Table 1 [19,20,38].

Table 1. Parameters of the two-dimensional wing.

Quasi-Steady Aerodynamic Model		Unsteady Aerodynamic Model	
Parameter	**Value**	**Parameter**	**Value**
m_{wing}	4.34 kg	m_{h}	6.815 kg
$m_{\text{W(total)}}$	5.23 kg	m_{α}	5.715 kg
m_{T}	15.57 kg	m_{β}	0.537 kg
s_p	0.5945 m	m_{γ}	0.5 kg
b	0.1905 m	I_{α}	0.119 kg·m^2
a	−0.6719	I_{β}	1×10^{-5} kg·m^2
c	0.381 m	I_{γ}	1×10^{-5} kg·m^2
$I_{\text{CG.wing}}$	0.04342 kg·m^2	r_{α}	0.040 m
I_{cam}	0.04697 kg·m^2	r_{β}	0
c_{h}	27.43 kg/s	r_{γ}	0
c_{α}	0.0360 kg·m^2/s	r_{ac}	−0.033 m
ρ	1.225 kg/m^3	$r_{3/4c}$	0.233 m
r_{cg}	−b(0.0998+a)	L_{β}	0.233 m
$C_{L\alpha}$	6.757	L_{γ}	-0.01 m
$C_{L\beta}$	3.774	$k_{\beta s}$	766.08 I_{β}
$C_{m\alpha}$	0	$c_{\beta s}$	41.82 I_{β}
$C_{m\beta}$	−0.6719	$k_{\gamma s}$	530.24 I_{γ}
$C_{L\gamma}$	−0.1566	$c_{\gamma s}$	44.27 I_{γ}
$C_{m\gamma}$	−0.1005	c_{α}	0.205 Nm·s/rad
k_{h}	2844 N/m	c_{h}	27.43 Nm·s/rad
x_{α}	r_{cg}/b m	$\omega_{n\beta s}$	27.68 rad/s
f_{LE}	0.15	$\zeta_{\beta s}$	0.7555
f_{TE}	0.2	$\omega_{n\gamma s}$	23.03 rad/s
I_{α}	$I_{\text{cam}} + I_{\text{CG.wing}} + m_{\text{wing}}(r_{\text{cg}})^2$ kg·m^2	$\zeta_{\gamma s}$	0.961
		k_{h}	2844 N/m
k_{α}	12.77 + 53.47α + 1003α^{2}Nm/rad	k_{α}	27.96 − 167.63α + 552.55α^2 + 1589.3α^3 − 3247.2α^4

4.1. Flutter Suppression

In this section, the flutter suppression of the airfoil is studied. For the two-dimensional airfoil, the polynomial model of the stiffness is found by static measurements on the nonlinear pitch cam, $k_\alpha(\alpha) = 12.77 + 53.47\alpha + 1003\alpha^2$ Nm/rad [19]. When the airspeed is increased to 11.4m/s, the LCO phenomenon appears. The output responses are shown in Figure 3. To suppress this LCO and flutter vibrations, different scenarios are studied. First, the proposed BTSMC is used to suppress this flutter. The initial conditions of the two-dimensional aeroelastic airfoil are as follows: $h(0) = -0.01$ m, $\alpha(0) = 0.1$ rad, $\dot{h}(0) = -0.1$ m/s, $\dot{\alpha}(0) = -2$ rad/s, and the nominal airspeed V = 11.4m/s. The parameters of the BTSMC are designed after several design iterations as follows: K_1 = diag(0.2,0.1), h_s = diag(0.5,0.5), ς = diag(30,45), $\varphi_s = 0.4$, $\beta_s = 1$, p = 5, $q = 3$, β = diag(1,1), $\alpha_0 = 10$, $\beta_1 = 3$, and $\lambda = 1.8$diag(1,1). The simulation results refer to Figure 4.

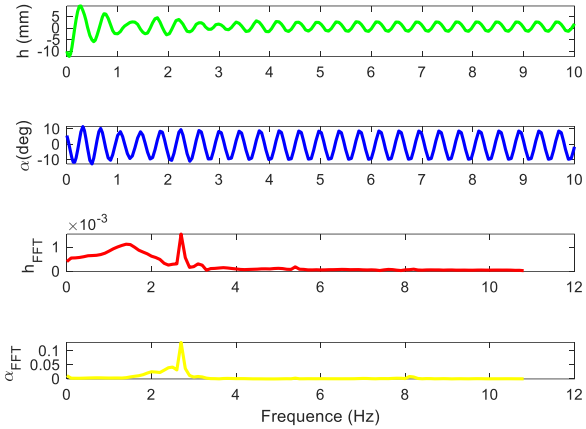

Figure 3. Responses of the open-loop system at the airspeed of V = 11.4 m/s.

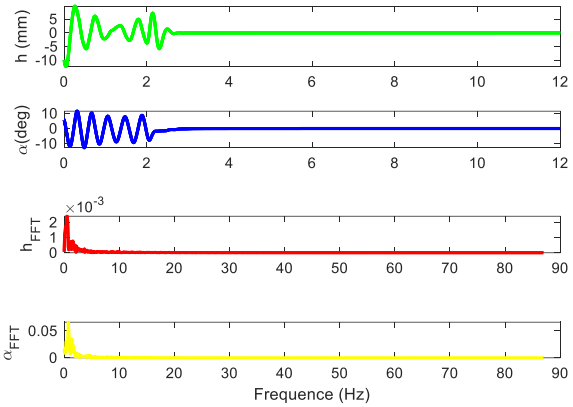

Figure 4. Output responses of plunge and pitch motions.

It can be seen from Figure 4 that the dynamic responses of the proposed nonlinear aeroelastic system flutter under the initial input during the first 2 s, and the resulting dynamic responses under the BTSMC are stable after 2 s. The FFT results of plunge displacements and AOA with and without BTSMC control are shown in Figures 3 and 4, the vibration frequency is 2.7 Hz (see Figure 3), and the amplitude of h_{FF} changes from 1.5×10^{-3} to 1.25×10^{-4}, while the amplitude of α_{FFT} changes from 0.1 to 7.4×10^{-3}, which shows that the flutter is suppressed by the proposed BTSMC.

For high stiffness nonlinearity in pitch, $k_\alpha(\alpha)$ can be modeled as the following polynomial type [20]:

$$k_\alpha = k_{\alpha 0} + k_{\alpha 1}\alpha + k_{\alpha 2}\alpha^2 + k_{\alpha 3}\alpha^3 + k_{\alpha 4}\alpha^4$$
$$= 27.96 - 167.63\alpha + 552.55\alpha^2 + 1589.3\alpha^3 - 3247.2\alpha^4$$

The flutter speed is related to its stiffness; the flutter equation for the *p*-*k* method can be written as follows using Equation (23) [39]:

$$\left[\left(\frac{V}{L_{ref}}\right)\mathrm{M}p^2 + \mathrm{K} - \frac{1}{2}\rho V^2\left(\mathrm{Q}^R(M,k) + \frac{p}{k}\mathrm{Q}^I(M,k)\right)\right]\cdot\{\mathrm{q}\} = 0. \tag{44}$$

where M and K are the generalized mass and stiffness matrices, respectively; $\mathrm{Q^R}$ and $\mathrm{Q^I}$ are the real and imaginary parts of the generalized aerodynamic force matrix that depends on Mach number M and reduced frequency k. V is the velocity of the undisturbed flow, and L_{ref} is the reference length. q denotes the eigenvector of the flutter equation; $p = g_s + i\omega_s$ is the non-dimensional Laplace complex parameter and is also referred to as an eigenvalue of Equation (44). The imaginary part of p must meet the following consistency condition: $k = \left(\frac{L_{ref}}{V}\right)\cdot \mathrm{Im}(p)$, i.e., $k = \left(\frac{L_{ref}}{V}\right)\cdot\omega$, and $\omega = \sqrt{\frac{\mathrm{K}}{\mathrm{M}}}$. When the damping curve {($\mathrm{V_s}$, $\mathrm{g_s}$)} for the vibration mode intersects with $\mathrm{g_s} = 0$, the associated speed is the flutter speed. Therefore, for a given k, when the stiffness K is increased, the frequency is increased, and the flutter speed $\mathrm{V_s}$ is increased. Here, the high stiffness is applied, and the flutter speed is increased from V = 11.4 m/s to V = 13.2 m/s. With this stiffness model, the simulation results are shown in Figures 5 and 6.

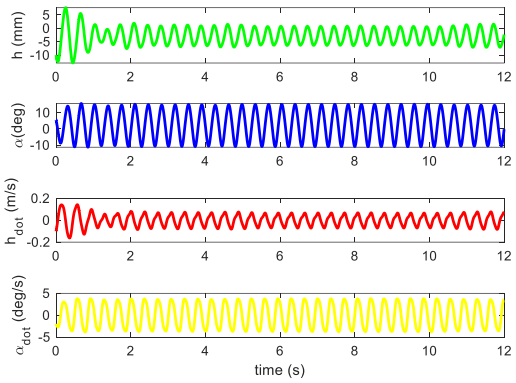

Figure 5. Output responses of plunge and pitch motions without control (high stiffness).

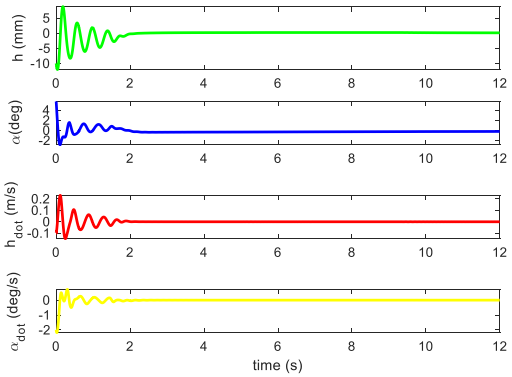

Figure 6. Output responses of plunge and pitch motions with control inputs (high stiffness).

It can be seen from Figures 5 and 6 that the flutter speed is increased from V = 11.4 m/s to V = 13.2 m/s by the high stiffness nonlinearity, and the output responses of the plunge and pitch motions rapidly converge with the proposed BTSMC control.

Considering a high angle of attack (AOA) in the post-flutter behavior, a square wave command of 10deg is tracked, and the output responses are shown in Figure 7.

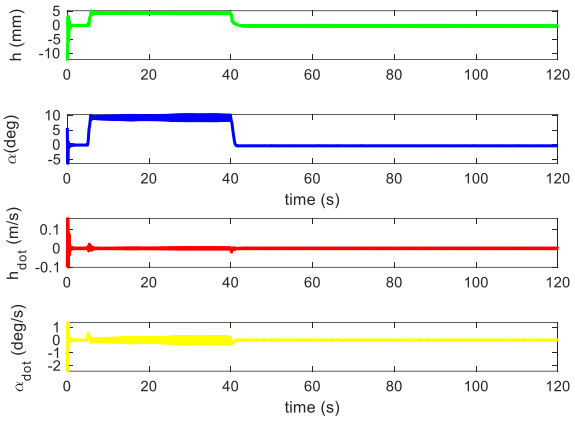

Figure 7. Output responses of plunge and pitch motions under 10deg AOA command.

It can be seen from Figure 7 that the 10° AOA command has been accurately tracked by the proposed BTSMC, but the control surfaces saturate, resulting in small oscillations of the output responses.

4.2. Flutter Suppression Under Unknown Wind Disturbances

Case I: for quasi-steady aerodynamic loads

There are two kinds of gusts to be studied here, that is, a triangular-type gust and a sine gust, as follows [30,36]:

$$w_G(\tau) = \begin{cases} 2w_0\frac{\tau}{\tau_G}\left(H(\tau) - H(\tau - \frac{\tau_G}{2})\right) + 2w_0\left(\frac{\tau}{\tau_G} - 1\right)\left(H(\tau - \tau_G) - H(\tau - \frac{\tau_G}{2})\right), & (\text{triangular gust}) \\ H(\tau)w_0\sin(0.5\tau), & (\text{sin e gust}) \end{cases}. \quad (45)$$

where $H(\cdot)$ denotes the Heaviside step function used to describe the typical velocity distribution time-history corresponding to the gust loads; this triangular gust lasts 0.5 s from t = 0 to t = 0.5 s, i.e., t_G = 0.05 s, w_0 = 0.3 m/s, $\tau_G = Vt_G/b$.

Where w_0 = 0.3 m/s, and this sine gust lasts 120 s from t = 0 to t = 120 s.

Note that the triangular gust is very similar to the traditional 1-cosine gust-type function, both of which can be classified as ephemeral disturbances. Since gusts will result in a lift force and pitch moment change, which then drive the vertical speed and pitch rate change, for simplification, we regard them as external disturbances by

$$\boldsymbol{D}(t) = \Gamma_w w_G(t) \quad (46)$$

where Γ_w is the gust effectiveness matrix, which can be approximated by Equations (29) and (30),

$$\Gamma_w = \left[-\rho(V + D_w)^2 b s_p C_{L\alpha}/(Vm_T) \quad \rho(V + D_w)^2 b^2 s_p C_{m\alpha}/(VI_\alpha)\right]^T, \quad (47)$$

The disturbance parameters of (31) are

$$W_d = \begin{bmatrix} 0 & 0.5 \\ -0.5 & 0 \end{bmatrix}, V_d = \begin{bmatrix} 2 & 0 \end{bmatrix}, \quad (48)$$

The associated DO gains of (33) are designed as follows:

$$l(h, \dot{h}) = \begin{bmatrix} 20 & 6 \end{bmatrix}^T, l(\alpha, \dot{\alpha}) = \begin{bmatrix} 5 & 0.4 \end{bmatrix}^T, (\text{forsinegust}) \quad (49)$$

$$l(h, \dot{h}) = \begin{bmatrix} 2.5 & 0.17 \end{bmatrix}^T, l(\alpha, \dot{\alpha}) = \begin{bmatrix} 5 & 0.4 \end{bmatrix}^T, (\text{fortriangulargust}) \quad (50)$$

Remark 2. *In this paper, single (1-cos) gusts (i.e., triangular gusts) and continuous sinusoidal (harmonic) gusts are considered. It can be seen from Equations (49) and (50) that the observer gains of l (h,ḣ) are different for different kinds of gusts, which shows that the DO is adaptive for the gusts. Different kinds of gusts can be detected by short-range light detection and ranging (Lidar) wind measurement.*

The parameter of the adaptive observer (Equation (A19)) is set as $\gamma_d = 0.2$. To illustrate our method in trajectory tracking control, a BSMC design from [40] is used for comparison. The sliding-mode surface is designed as

$$\boldsymbol{s} = \boldsymbol{\lambda}_1 \boldsymbol{z}_1 + \boldsymbol{z}_2 \tag{51}$$

and the BSMC controller is designed as follows:

$$\boldsymbol{U}_{BSMC} = (g_2)^{-1}\left(-(K_1 + \lambda_1)\dot{\boldsymbol{z}}_1 - f_2 + \ddot{\boldsymbol{x}}_{1d} - \hat{\boldsymbol{d}} - (h\boldsymbol{s} + \varsigma \mathrm{sgn}(\boldsymbol{s}))\right) \tag{52}$$

A PID controller is applied as follows:

$$\boldsymbol{U}_{\mathrm{PID}} = (g_2)^{-1}\left(-(K_{p,z_1}\boldsymbol{z}_1 + K_{I,z_1}\int_0^t \boldsymbol{z}_1 dt) - (K_{p,z_2}\boldsymbol{z}_2 + K_{I,z_2}\int_0^t \boldsymbol{z}_2 dt) - f_2 + \ddot{\boldsymbol{x}}_{1d} - \hat{\boldsymbol{d}}\right) \tag{53}$$

The parameters of the studied controllers are designed as shown in Table 2 after several design iterations.

Table 2. Selected parameters of the controller (quasi-steady case).

Controller	Parameters	Value
PID	$k_{p,z1}$, $k_{i,z1}$, $k_{p,z2}$, $k_{i,z2}$	diag(0.1,0.1), diag(0.1,0.1), diag(1,1), diag(0.4,0.4)
BTSMC		The same as Section 4.1
BSMC	K_1, λ_1	diag(0.4,0.2), diag(0.5,0.5)
	h_s, ς	diag(0.5,0.5), diag(50, 30)
	φ_s, β_s	0.4, 1

The simulation results using the proposed DO-BTSMC, BSMC, and PID design are shown in Figures 8–14 and Tables 3 and 4.

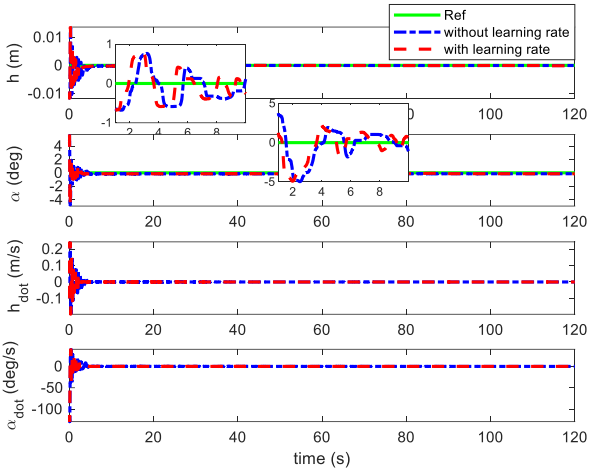

Figure 8. Responses of plunge and pitch under triangular gust with quasi-steady aerodynamic loads.

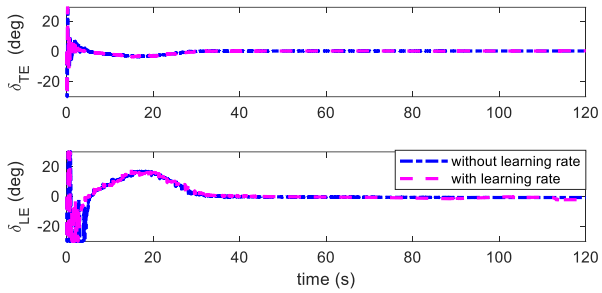

Figure 9. Deflection of TE and LE control under triangular gust with quasi-steady aerodynamic loads.

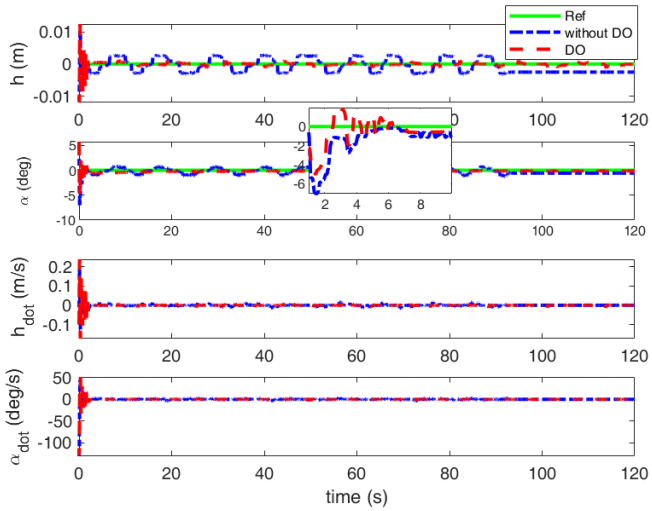

Figure 10. Output responses of plunge and pitch under sine gust with quasi-steady aerodynamic loads.

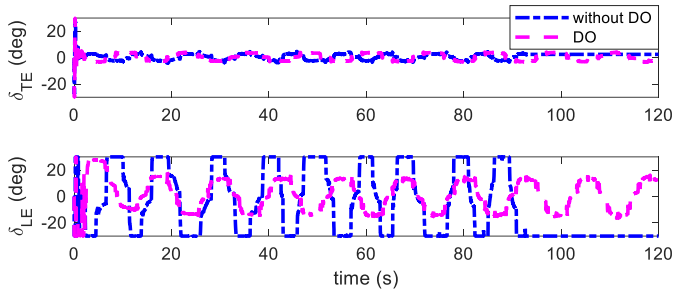

Figure 11. Deflection of TE and LE control under sine gust with quasi-steady aerodynamic loads.

Table 3. Performance data comparison under triangular and sine gusts.

Gust Input	Controller	Data	Rising Time (s)	Over-Shoots	RMSE
Triangular gust (Case I, Example 1)	No LR (with DO)	h	0.1770	0.0134	0.0023
		α	–	–	0.0129
	LR (with DO)	h	0.1187	0.0136	0.0022
		α	–	–	0.0120
Sine gust (Case I, Example 2)	No DO (No LR)	h	0.1084	0.0104	0.0027
		α	–	–	0.0160
	DO (No LR)	h	0.1205	0.0124	0.0018
		α	–	–	0.0110

'–' denotes a non-statistical variable in Table 3.

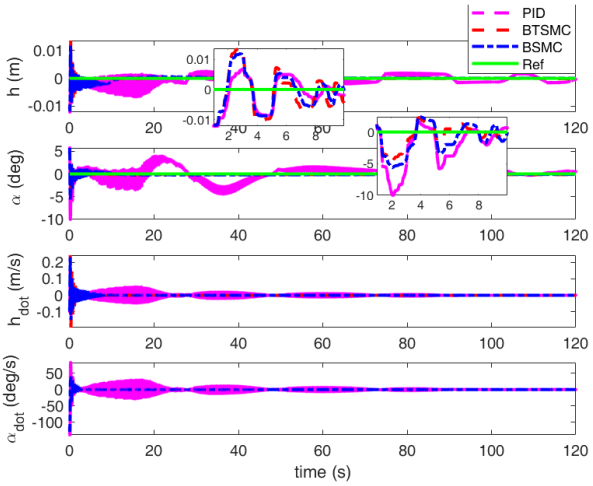

Figure 12. Responses of plunge and pitch under triangular gust with quasi-steady aerodynamic loads.

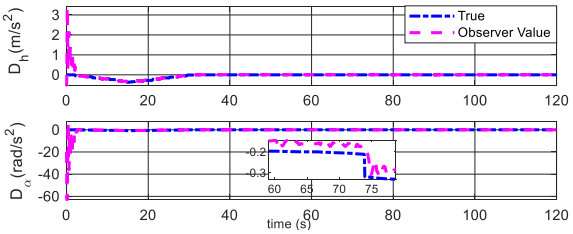

Figure 13. Observable disturbance estimation under triangular gust.

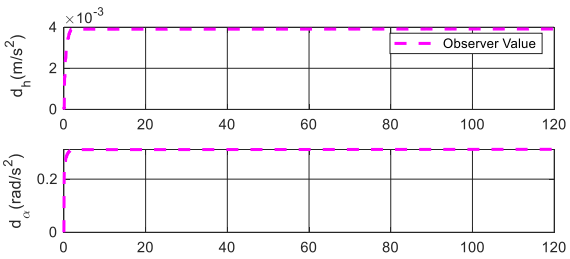

Figure 14. Unobservable disturbance estimation under triangular gust.

Table 4. Performance data comparison under triangular gust (quasi-steady aerodynamic loads).

Controller	Variant	Rising Time (s)	Over-Shoots	RMSE
DO-PID	h	0.1467	0.0067	0.0026
	α	-	-	0.0345
DO-BTSMC	h	0.1187	0.0136	0.0021
	α	-	-	0.0120
DO-BSMC	h	0.1215	0.0118	0.0022
	α	-	-	0.0153

Example 1. *Firstly, we consider different cases of the BTSMC design with and without the learning rate α_r under the triangular gust of (45), and the DO is applied; the output responses are shown in Figures 8 and 9 and Table 3, where the reference inputs of root mean square error (RMSE) are $h_{cmd} = 0$ and $\alpha_{cmd} = 0$.*

Example 2. *Secondly, we consider the case of the BTSMC design with and without a DO under the sine gust of (45), and there is no learning rate; the output responses are shown in Figures 10 and 11 and Table 3.*

Considering a triangular gust input, it can be seen from Figures 8 and 9 and Table 3 that the resulting dynamic responses of the proposed nonlinear aeroelastic system are stable, and the rise time of plunge responses for BTSMC with a learning rate and DO is shorter than that of the BTSMC without a learning rate but with a DO, which shows the tracking speed of the BTSMC with a learning rate for the plunge motions is faster than that of the BTSMC without a learning rate, but the LR can produce small overshoots; see Figure 8. The root mean square errors of the plunge and pitch motion for the BTSMC with an LR and a DO are smaller than those for the BTSMC without an LR. This shows the learning rate of the BTSMC can improve the control performance.

Now considering a sine gust input, Figures 10 and 11 and Table 3 show that the resulting dynamic responses of the proposed nonlinear aeroelastic system are stable, and the steady-state errors of the BTSMC with a DO for the plunge and pitch motions are less than those of the BTSMC without a DO. The associated control inputs for the LE control surface are smaller than for the BTSMC without a DO. This shows the disturbance observer of (32) and (A19) can effectively estimate an unknown time-varying gust, and the disturbance compensator reduces the disturbance effect for the aeroelastic system.

Finally, we consider the different flutter suppression approaches of the BTSMC, BSMC, and PID under the triangular gust of Equation (45). The output responses obtained by using the proposed design with the DO of (32) and an adaptive observer (Equation (A19)) are shown in Table 4 and Figures 12–14. The sign function of the SMC design is replaced by the tangent hyperbolic function with a boundary layer (where $\varphi_s = 0.4$).

It can be seen from Figure 12 and Table 4 that the resulting dynamic responses of the proposed nonlinear aeroelastic system are convergent to the desired values, and the rise time of plunge responses for DO-BTSMC is shorter than that of the DO-BSMC and DO-PID control, which shows that the BTSMC response is the fastest among them. The output responses of the PID control easily oscillate under triangular gusts while the responses of the BTSMC and BSMC design are steady after the transition process, which shows the robust performances of the BTSMC and BSMC. The root mean square errors of the plunge and pitch motion for the DO-BTSMC are the smallest, while those for the PID control are the highest, and RMSEs for the DO-BSMC are between them, showing that the tracking precision is the highest for the DO-BTSMC, second highest for the DO-BSMC, and worst for the PID control. Figure 10 shows that the triangular gust of (45) can be effectively estimated and that the unobservable disturbances including uncertainties are estimated by the adaptive observer (Equation (A19)) (see Figure 14), which reduces the effect of a triangular gust on the aeroelastic system.

Case II: for unsteady aerodynamic load.

As the post-flutter behavior of the airfoil is intrinsically unsteady, the unsteady aerodynamic loads are calculated by Equations (10)–(27), and the parameters of the studied controllers are designed as shown in Table 5 after several design iterations.

The associated DO gains of Equation (33) are designed as follows:

$$l(h,\dot{h}) = \begin{bmatrix} 25 & 0.25 \end{bmatrix}^T, l(\alpha,\dot{\alpha}) = \begin{bmatrix} 50 & 0.4 \end{bmatrix}^T, l(\beta,\dot{\beta}) = \begin{bmatrix} 0.5 & 0.04 \end{bmatrix}^T, l(\gamma,\dot{\gamma}) = \begin{bmatrix} 0.5 & 0.04 \end{bmatrix}^T, \quad (54)$$
(forsinegust)

$$l(h,\dot{h}) = \begin{bmatrix} 25 & 0.25 \end{bmatrix}^T, l(\alpha,\dot{\alpha}) = \begin{bmatrix} 50 & 0.4 \end{bmatrix}^T, l(\beta,\dot{\beta}) = \begin{bmatrix} 5 & 0.4 \end{bmatrix}^T, l(\gamma,\dot{\gamma}) = \begin{bmatrix} 5 & 0.4 \end{bmatrix}^T, \quad (55)$$
(fortriangulargust)

Table 5. Selected parameters of the controller (unsteady case).

Controller	Parameters	Value
PID	$k_{p,z1}$, $k_{i,z1}$, $k_{p,z2}$, $k_{i,z2}$	diag(0.1,0.1,0.1,0.1), diag(0.1,0.1,0.1,0.1), diag(1,1,1,1), diag(0.4,0.4, 0.4, 0.4)
BTSMC	K_1, λ_1	K_1 = diag(0.2,0.1,0.1,0.1), $\lambda = 1.8 \times$ diag(1,1,1,1).
	p, q	5, 3
	β, α_0, β_1	β = diag(1,1,1,1), $\alpha_0 = 10$, $\beta_1 = 3$,
	h_s, ς	h_s = diag(0.5,0.5,0.5,0.5), ς = diag(30,50, 30, 30),
	φ_s, β_s	$\varphi_s = 0.4$, $\beta_s = 1$
BSMC	K_1, λ_1	diag(0.2,0.1,0.1,0.1), diag(0.5,0.5,0.5,0.5)
	h_s, ς	diag(0.5,0.5,0.5,0.5), diag(30,50, 30, 30)
	φ_s, β_s	0.4, 1

Example 3. *Firstly, we consider the different cases for the BTSMC design with and without the learning rate α_r under the triangular gust of (45), and the external disturbances given by Equation (46), where Γ_w is the gust effectiveness matrix, which can be approximated as*

$$\Gamma_w = \left[-\rho(V + D_w)^2 bC_{L\alpha}/(Vm_T) \quad M_D \quad M_D/2 \quad M_D/2\right]^T \tag{56}$$

where $M_D = \rho(V + D_w)^2 b^2 s_p C_{m\alpha}/(VI_\alpha)$, the disturbance parameters are the same as those in Example 1 with w_0 = 3 m/s, and the DO is applied; the output responses are shown in Figures 15–17.

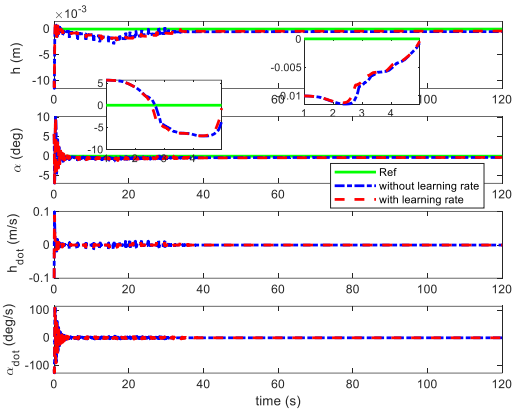

Figure 15. Responses of plunge and pitch under triangular gust with unsteady aerodynamic loads.

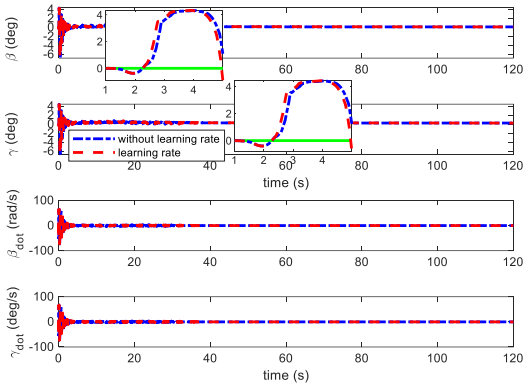

Figure 16. Responses of β and γ under triangular gust with unsteady aerodynamic loads.

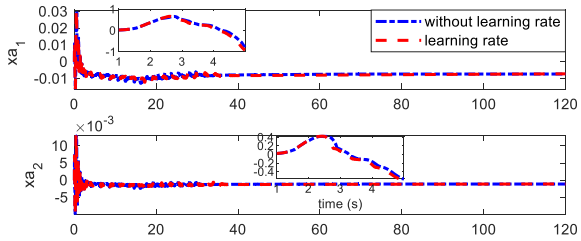

Figure 17. Responses of aerodynamic states under triangular gust with unsteady aerodynamic loads.

The control inputs are shown in Figure 18.

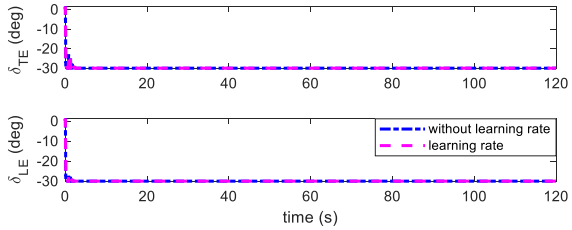

Figure 18. Deflection of TE and LE control under triangular gust with unsteady aerodynamic loads.

The wind disturbances are estimated by the proposed DO (32) and are shown in Figure 19.

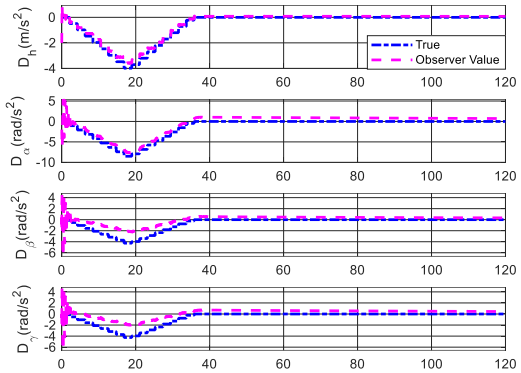

Figure 19. Disturbance estimation under triangular gust by DO.

Example 4. *Secondly, we consider the case of the BTSMC design with and without a DO under the sine gust of (45); the disturbance parameters are the same as those for Example 2, and there is no learning rate. The output responses are shown in Figures 20–23 and in Table 6.*

Table 6. Performance data comparison under triangular and sine gusts with unsteady aerodynamic loads.

Gust Input	Controller	Data	Rising Time (s)	Over-Shoots	RMSE
Triangular gust (Case II, Example 3)	No LR (with DO)	h	0.2438	0.0010	0.0022
		α	-	0.1758	0.0285
	LR (with DO)	h	0.2278	0.0015	0.0020
		α	-	0.1782	0.0281
Sine gust (Case II, Example 4)	No DO (No LR)	h	0.1704	0.0045	0.0019
		α	-	0.2312	0.0267
	DO (No LR)	h	0.1447	0.0025	0.0013
		α	-	0.2144	0.0218

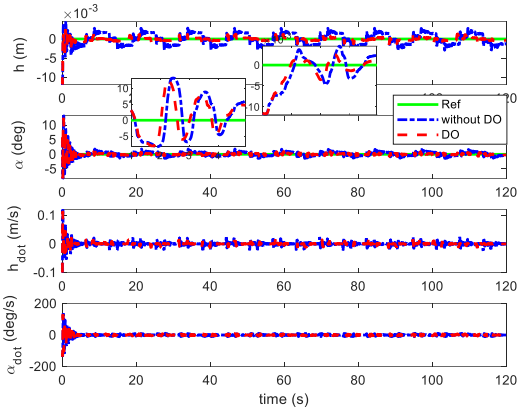

Figure 20. Output responses of plunge and pitch under sine gust with unsteady aerodynamic loads.

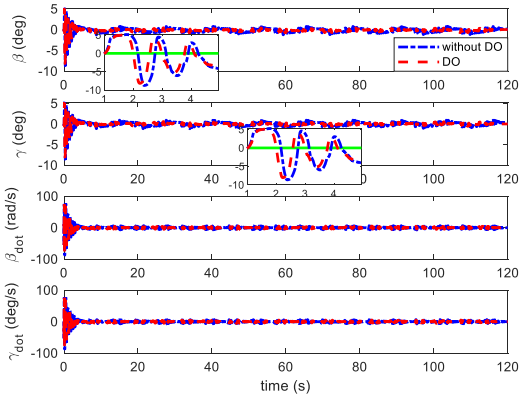

Figure 21. Responses of β and γ under sine gust with unsteady aerodynamic loads.

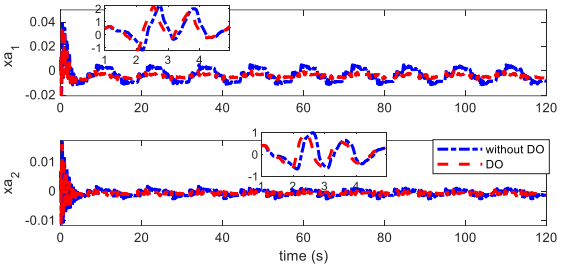

Figure 22. Responses of aerodynamic states under sine gust with unsteady aerodynamic loads.

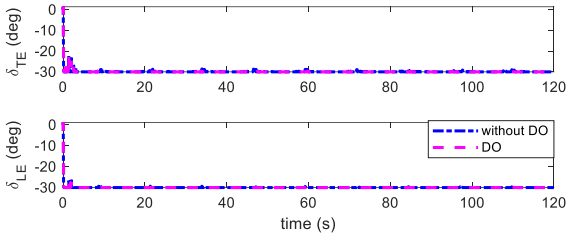

Figure 23. Deflection of TE and LE control under sine gust with unsteady loads.

The control inputs refer to Figure 23.

Considering the triangular gust input, it can be seen from Figures 15–17 and Table 6 that the resulting dynamic responses of the proposed nonlinear aeroelastic system are stable, and the rise time of plunge responses for BTSMC with LR and DO is shorter than that of for the BTSMC without an LR but with a DO, which shows the tracking speed of the

BTSMC with a learning rate and DO for the plunge motions is faster than that of the BTSMC without a learning rate, but the LR can produce a small overshoot; see Figures 15–17. The RMSE of the plunge and pitch motion for the BTSMC with a learning rate and DO is smaller than that of the BTSMC without an LR. This shows the learning rate of the BTSMC can improve the control performances.

Now consider the sine gust input. Figures 20–23 and Table 3 show that the resulting dynamic responses of the proposed nonlinear aeroelastic system are stable, and the steady-state errors of the BTSMC with a DO for the plunge and pitch motions are less than those of the BTSMC without a DO, and the associated control inputs are smaller than those of the BTSMC without a DO. This shows the disturbance observer of (32) and (A19) can effectively estimate an unknown time-varying gust and that the disturbance compensator reduces the disturbance effect for the aeroelastic system. Figure 19 shows that the external disturbances can be estimated quickly and accurately.

4.3. Robust Flutter Suppression with Parameter Uncertainties and Disturbances

Case I: for quasi-steady aerodynamic loads

Example 5. *Consider the effect of parameter uncertainties on the aeroelastic system. The parameter uncertainties of k_h, k_α, and c_h are set to be $\pm 1\%$, and the uncertainties of c_α and $C_{L\alpha}$ are set to be $\pm 30\%$ and $\pm 7\%$, respectively. The external disturbance is set as the sine gust of (45). The controller parameters are designed and listed in Table 2, and the sign function of the SMC design is replaced by a continuous approximation of the sign function $sgn(s) \approx s/\sqrt{s^T s + \beta_s}$ with $\beta_s = 1$. Since the DO-BTSMC can deal with model uncertainties through adaptive disturbance estimation and gain regulation, we use the proposed DO-BTSMC design, and the simulation results are shown in Table 7 and Figures 24–27.*

Table 7. Performance data comparison under parameter uncertainty and sine gust (quasi-steady case).

Controller	Variant	Rising Time (s)	Over-Shoots	RMSE
DO-PID	h	0.1481	0.0077	0.0025
	α	-	-	0.0447
DO-BTSMC	h	0.1205	0.0124	0.0018
	α	-	-	0.0110
DO-BSMC	h	0.1275	0.0045	0.0014
	α	-	-	0.0173

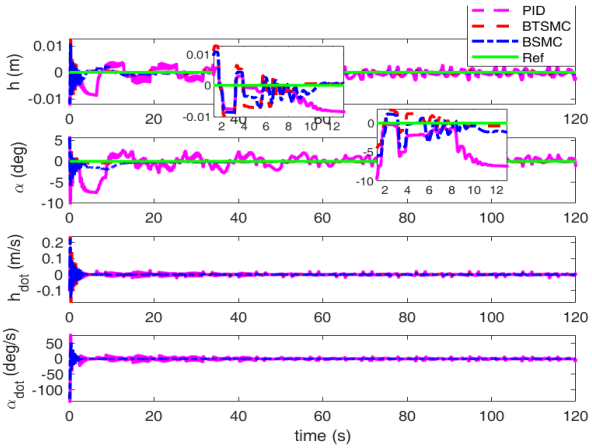

Figure 24. Responses of plunge and pitch under sine gust with quasi-steady aerodynamic loads.

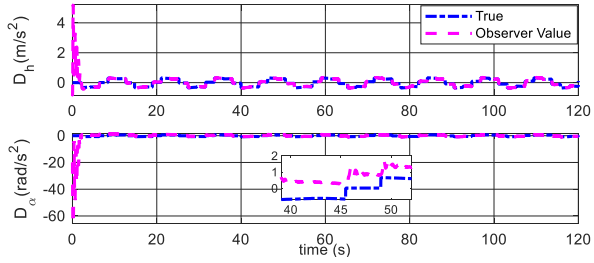

Figure 25. Observable disturbance estimation under sine gust with quasi-steady aerodynamic loads.

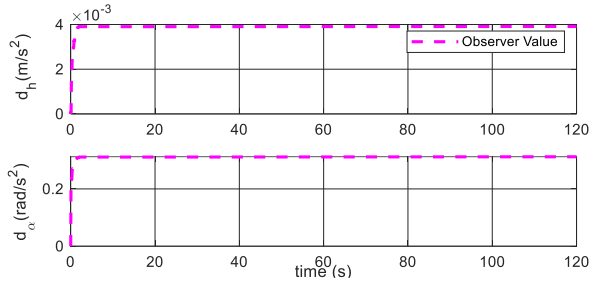

Figure 26. Unobservable disturbance estimation under sine gust with quasi-steady aerodynamic loads.

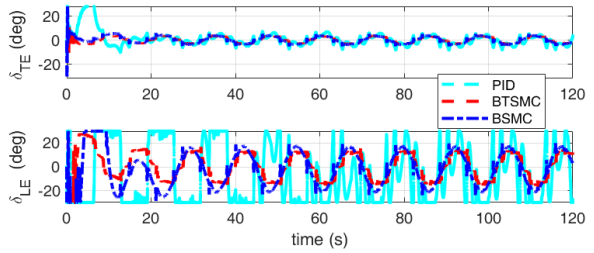

Figure 27. Deflection of TE and LE control under sine gust with quasi-steady aerodynamic loads.

It can be seen from Figure 24 and Table 7 that the resulting dynamic responses of the proposed nonlinear aeroelastic system are convergent, and the rise time of plunge responses for DO-BTSMC is the shortest. This shows that the BTSMC response is the fastest among them and demonstrates the DO-BTSMC has a fast transient response and finite time-convergence. But the BTSMC produces larger overshoots than the BSMC and PID designs. This is because larger inputs are required for finite-time convergence during the transition process for the DO-BTSMC. The RMSEs of the plunge and pitch motion show that the tracking precision of the DO-BTSMC is the best, followed by DO-BSMC and then the PID control. Meanwhile, the output responses of the PID control are vibrating under the sine gust, which shows that the robust performance of the PID controller is poorer than that of the BTSMC and BSMC. Figure 25 shows that the sine gust of Equation (45) can be effectively estimated, and the unobservable disturbances are also estimated by the adaptive observer of (Equation (A19)) as shown in Figure 26, which reduces the effect of the sine gust on the aeroelastic system. Figure 27 shows that the control surface deflections of the DO-BTSMC are the smallest and fastest, but the control inputs of the DO-PID control are the largest and easily cause control surface saturation; this also demonstrates the robust performances of the BTSMC.

Case II: for unsteady aerodynamic load

Example 6. *For unsteady aerodynamic loads with disturbances and model parameter uncertainties, the parameters of disturbances and uncertainties are the same as those for Example 5, and we use the proposed DO-BTSMC design. The simulation results are shown in Table 8 and Figures 28–33.*

Table 8. Performance data comparison under parameter uncertainty and sine gust (unsteady case).

Controller	Variant	Rising Time (s)	Over-Shoots	RMSE
DO-PID	h	0.1916	0.0024	0.0017
	α	-	0.2137	0.0199
DO-BTSMC	h	0.1415	0.0025	0.0010
	α	-	0.2147	0.0183
DO-BSMC	h	1.3885	0.0004	0.0010
	α	-	0.1645	0.0151

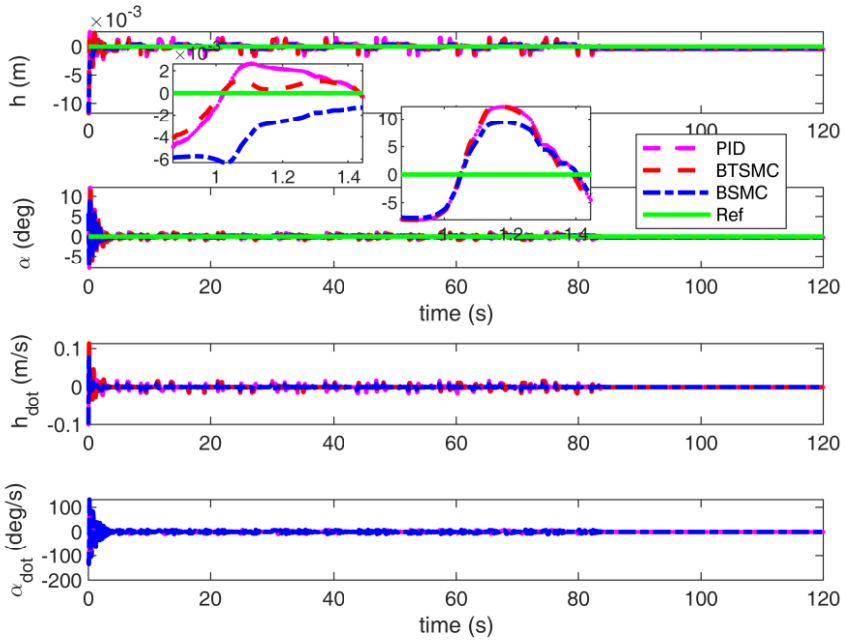

Figure 28. Responses of plunge and pitch under sine gust with unsteady aerodynamic loads.

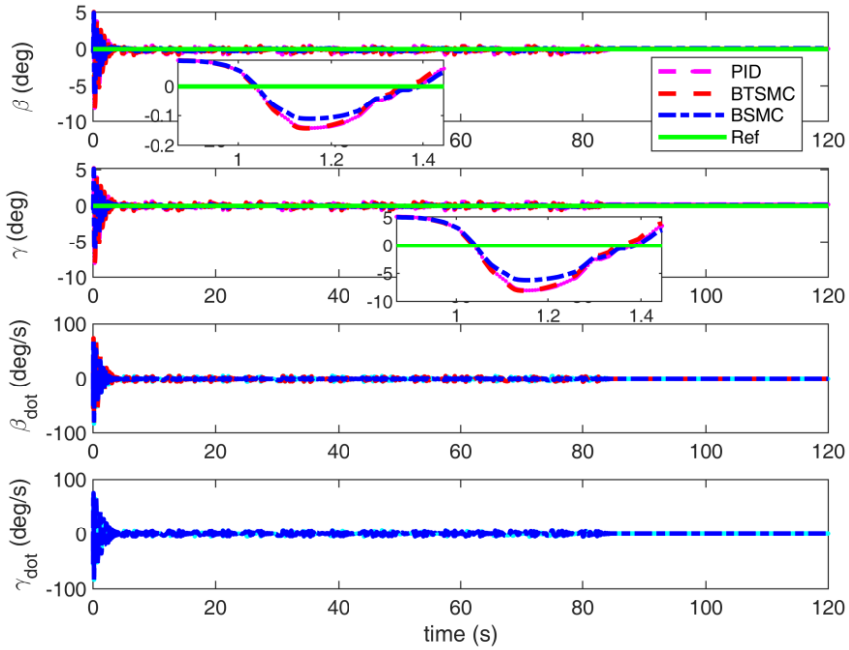

Figure 29. Responses of β and γ under sine gust with unsteady aerodynamic loads.

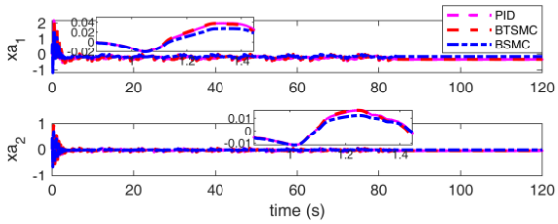

Figure 30. Responses of aerodynamic states under sine gust with unsteady aerodynamic loads.

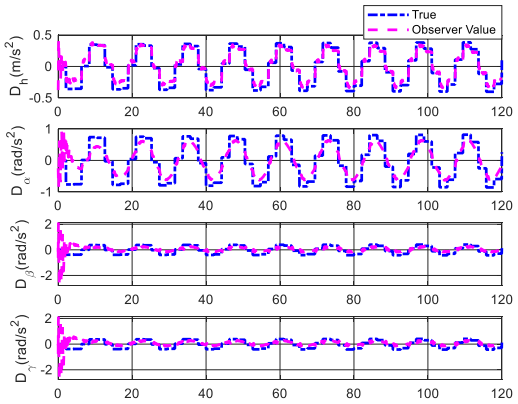

Figure 31. Observable disturbance estimation under sine gust with unsteady aerodynamic loads.

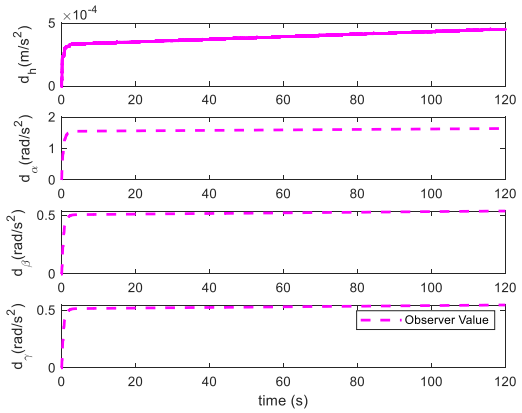

Figure 32. Unobservable disturbance estimation under sine gust with unsteady aerodynamic loads.

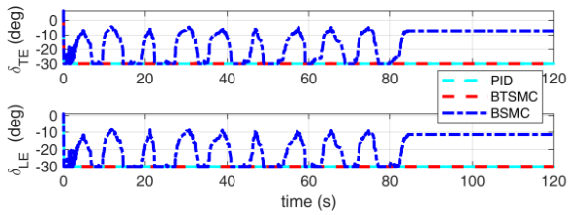

Figure 33. Deflection of TE and LE control under sine gust with unsteady aerodynamic loads.

It can be seen from Figures 28–30 and Table 8 that the resulting dynamic responses of the proposed nonlinear aeroelastic system are convergent, and the rise time of plunge responses for DO-BTSMC is the shortest, which shows the BTSMC response is the fastest and shows that the DO-BTSMC has a fast transient response and finite-time convergence. But the BTSMC produces larger overshoots than the BSMC and the PID design. This is because a larger input is required for finite-time convergence during the transition process for the DO-BTSMC. The root mean square errors of the plunge and pitch motion for the

DO-BTSMC are 0.0010 m and 0.0183 rad, respectively, and those for the DO-BSMC are 0.0010 m and 0.0151 rad respectively, while those for the PID control are 0.0017 m and 0.0199 rad, respectively, which shows that the tracking precision of the DO-BSMC is the best, followed by the DO-BTSMC and then the PID control. Although the tracking precision of the DO-BSMC is better than that of the DO-BTSMC, the rise time of the plunge motion response for DO-BSMC is very slow, which shows its vulnerability to damping.

The disturbance can be estimated by the proposed DO Equations (32) and (A19); the outputs are shown in Figures 31 and 32.

The control inputs refer to Figure 33.

Figure 31 shows that the sine gust of (45) can be effectively estimated and the unobservable disturbances are also estimated by the adaptive observer of (A19) as shown in Figure 32, which reduces the effect of the sine gust on the aeroelastic system. Figure 33 shows that the control surface deflections of DO-BTSMC are the smallest and fastest. In addition, the control inputs of the DO-BSMC control are the largest and easily cause control surface saturation; this also demonstrates the DO-BSMC has small damping and reduced tracking performance.

5. Conclusions

A nonlinear backstepping nonsingular terminal SMC method is used to design a controller to suppress limit cycle oscillation (LCO) and flutter. The developed controller stabilizes the plunge and pitch motions of the two-dimensional airfoil with LE and TE control surfaces with finite-time convergence. Stability analysis shows that the closed-loop aeroelastic dynamics are globally asymptotically stable. Six examples with variable bounded disturbances of triangular gust and sine gust and model parameter uncertainties are simulated. Compared with the BSMC and PID controllers, the DO-BTSMC with a learning rate achieves better flutter suppression performances with a fast response (improved by 18.6%) and reduced root mean square error (by 75% for α). Therefore, the effectiveness and availability of the DO-BTSMC design are demonstrated.

Author Contributions: Conceptualization, S.L. and J.F.W.; methodology, S.L., C.Y. and Q.Z.; software, S.L. and C.Y.; validation, S.L., J.F.W. and Q.Z.; formal analysis, J.F.W.; investigation, S.L. and Q.Z.; writing—original draft preparation, S.L.; writing—review and editing, S.L. and J.F.W.; visualization, S.L.; supervision, J.F.W. All authors have read and agreed to the published version of the manuscript.

Funding: This research was funded by the National Natural Science Foundation of China (No. 52272400 and No. 10577012), which we gratefully acknowledge.

Data Availability Statement: Sample data available on request.

Conflicts of Interest: The authors declare no conflicts of interest.

Appendix A. Aeroelastic Controller Design

Substituting (40) and (42) into (39) yields

$$\dot{z}_1 = z_2 + \phi_1(x_1) - \dot{x}_{1d} = z_2 - K_1 z_1 \tag{A1}$$

that is,

$$z_2 = \dot{z}_1 + K_1 z_1. \tag{A2}$$

Differentiating (A2) and substituting (38) yields

$$\dot{z}_2 = \ddot{x}_1 - \ddot{x}_{1d} + K_1 \dot{z}_1. \tag{A3}$$

From (40) and (A1), the derivative of the stabilizing function $\phi_1(x)$ is

$$\dot{\phi}_1(x_1) = \ddot{x}_{1d} - K_1(z_2 - K_1 z_1) = \ddot{x}_{1d} - K_1 z_2 + K_1^2 z_1. \tag{A4}$$

The derivative of the first CLF of (41) can be rewritten as follows by substituting (A1):

$$\dot{V}_1 = z_1^T \dot{z}_1 = z_1^T (z_2 - K_1 z_1) = -z_1^T K_1 z_1 + z_1^T z_2. \tag{A5}$$

Now a nonsingular terminal sliding-mode (NTSM) surface with a learning rate is designed by using the fractional order derivative as follows [41]:

$$\boldsymbol{s} = z_1 + \alpha_\gamma z_1^{\lambda} + \frac{1}{\beta} z_2{}^{p/q} = z_1 + \alpha_\gamma |z_1|^{\lambda} \mathrm{sgn}(z_1) + \frac{1}{\beta} |z_2|^{p/q} \mathrm{sgn}(z_2) \tag{A6}$$

where $s = \begin{bmatrix} s_1 & s_2 \end{bmatrix}^T \in R^2$ denotes sliding-mode surface, $1 < p/q < 2$, $i = 1,2$, sgn(.) is sign function, and the SMC parameter $\lambda > p/q$.

To adjust the speed of the aeroelastic responses converging to zero, a learning rate is proposed as follows:

$$\alpha_\gamma = \alpha_0 + \alpha_1 \left| \dot{z}_1(t) \right|, \tag{A7}$$

where α_1 is the learning rate, which is defined as $\alpha_1 = \beta_1^{|\dot{z}_1(t)|} - 1$; α_0 is a positive constant, $\beta_1 > 0$, and $\beta_1 \neq 1$. So the derivative of sliding-mode surface s of Equation (A6) obtained by using Equation (A3) is as follows:

$$\dot{\boldsymbol{s}} = \dot{z}_1 + \alpha_\gamma \lambda |z_1|^{\lambda-1} \cdot \dot{z}_1 + \frac{1}{\beta} \cdot \frac{p}{q} |z_2|^{(p/q-1)} \cdot \dot{z}_2 = \dot{z}_1 + \alpha_\gamma \lambda |z_1|^{\lambda-1} \cdot \dot{z}_1 + \frac{1}{\beta} \cdot \frac{p}{q} |z_2|^{(p/q-1)} \left(\ddot{x}_1 - \ddot{x}_{1d} + K_1 \dot{z}_1 \right) \tag{A8}$$

The candidate CLF is redefined as

$$V_2 = V_1 + \frac{1}{2} \boldsymbol{s}^T \boldsymbol{s} + \frac{1}{2\gamma_d} \widetilde{\boldsymbol{d}}^T \widetilde{\boldsymbol{d}}, \tag{A9}$$

where γ_d is a positive constant that determines the convergence speed of the estimate. Differentiating (A9) yields

$$\dot{V}_2 = z_1^T \dot{z}_1 + \boldsymbol{s}^T \dot{\boldsymbol{s}} + \frac{1}{\gamma_d} \widetilde{\boldsymbol{d}}^T \dot{\widetilde{\boldsymbol{d}}} \tag{A10}$$

Since $\boldsymbol{d}$ is an unknown constant or slow-varying disturbance, the derivative of the estimated parameter error is

$$\dot{\widetilde{\boldsymbol{d}}} = \dot{\hat{\boldsymbol{d}}} - \dot{\boldsymbol{d}} = \dot{\hat{\boldsymbol{d}}}. \tag{A11}$$

where $\hat{d}$ and $\widetilde{d}$ are the estimated parameter vector of d and the associated estimated parameter error vector. Substituting (37), (A5), (A8), and (A11) into (A10) yields

$$\begin{aligned} \dot{V}_2 &= z_1^T \dot{z}_1 + \boldsymbol{s}^T \dot{\boldsymbol{s}} + \tfrac{1}{\gamma_d} \widetilde{\boldsymbol{d}}^T \dot{\widetilde{\boldsymbol{d}}} \\ &= -z_1^T K_1 z_1 + z_1^T z_2 + \tfrac{1}{\gamma_d} \widetilde{\boldsymbol{d}}^T \dot{\hat{\boldsymbol{d}}} + \boldsymbol{s}^T \left(\dot{z}_1 + \alpha_\gamma \lambda \left| z_1 \right|_{\lambda-1} \cdot \dot{z}_1 + \tfrac{1}{\beta} \cdot \tfrac{p}{q} z_2{}^{(p/q-1)} \left(\ddot{x}_1 - \ddot{x}_{1d} + K_1 \dot{z}_1 \right) \right) \\ &= -z_1^T K_1 z_1 + z_1^T z_2 + \tfrac{1}{\gamma_d} \widetilde{\boldsymbol{d}}^T \dot{\hat{\boldsymbol{d}}} + \boldsymbol{s}^T \left((z_2 - K_1 z_1) \left(1 + \alpha_\gamma \lambda |z_1|^{\lambda-1} \right) + \tfrac{1}{\beta} \cdot \tfrac{p}{q} z_2{}^{(p/q-1)} \left(\ddot{x}_1 - \ddot{x}_{1d} + K_1 \dot{z}_1 \right) \right) \\ &= z_1^T (-K_1 z_1 + z_2) + (\mathrm{I}_n + \alpha_\gamma \lambda \mathrm{diag}(|z_{1,i}|_{\lambda-1})) (\boldsymbol{s}^T z_2 - K_1 z_1^T \boldsymbol{s}) \\ &+ \tfrac{1}{\gamma_d} \widetilde{\boldsymbol{d}}^T \dot{\hat{\boldsymbol{d}}} + \boldsymbol{s}^T \left(\tfrac{1}{\beta} \cdot \tfrac{p}{q} z_2{}^{(p/q-1)} \left(f_2 + g_2 \boldsymbol{U}_{BTSMC} + K_1 \dot{z}_1 - \ddot{x}_{1d} + \boldsymbol{d} \right) \right) \end{aligned} \tag{A12}$$

A desired control input is selected as follows to make (A12) semi-negative definite:

$$\boldsymbol{U}_{BSMC} = g_2^{-1} \left(-\beta \cdot \frac{q}{p} z_2{}^{(2-p/q)} - K_1 \dot{z}_1 - f_2 + \ddot{x}_{1d} - \hat{\boldsymbol{d}} - (h_s \boldsymbol{s} + \varsigma \mathrm{sgn}(\boldsymbol{s})) \right) \tag{A13}$$

as

$$\begin{aligned}
&z_1^T(-K_1z_1+z_2)-(\mathrm{I}_n+\alpha_\gamma\lambda\mathrm{diag}(|z_{1,\mathrm{i}}|_{\lambda-1}))K_1z_1^T\boldsymbol{s}\\
&=-K_1z_1^Tz_1+z_1^Tz_2-(\mathrm{I}_n+\alpha_\gamma\lambda\mathrm{diag}(|z_{1,\mathrm{i}}|_{\lambda-1}))K_1z_1^T\left(z_1+\tfrac{1}{\beta}z_2{}^{p/q}\right)\\
&=-K_1z_1^Tz_1+z_1^Tz_2-(\mathrm{I}_n+\alpha_\gamma\lambda\mathrm{diag}(|z_{1,\mathrm{i}}|_{\lambda-1}))K_1z_1^T\left(z_1+\alpha_\gamma z_1^\lambda+\tfrac{1}{\beta}z_2{}^{p/q}\right)\\
&=-K_1z_1^Tz_1+z_1^Tz_2-(\mathrm{I}_n+\alpha_\gamma\lambda\mathrm{diag}(|z_{1,\mathrm{i}}|_{\lambda-1}))(K_1z_1^Tz_1+\alpha_\gamma K_1z_1^Tz_1^\lambda)\\
&-\tfrac{1}{\beta}(\mathrm{I}_n+\alpha_\gamma\lambda\mathrm{diag}(|z_{1,\mathrm{i}}|_{\lambda-1}))K_1z_1^Tz_2{}^{p/q}\\
&=-(2\mathrm{I}_n+\alpha_\gamma\lambda\,|\mathrm{diag}\,(|z_{1,\mathrm{i}}|_{\lambda-1}))K_1z_1^Tz_1+z_1^Tz_2-(\mathrm{I}_n+\alpha_\gamma\lambda\mathrm{diag}(|z_{1,\mathrm{i}}|_{\lambda-1}))\\
&\cdot\alpha_\gamma K_1\left|z_1\right|_{\lambda-1}z_1^Tz_1-\tfrac{1}{\beta}(\mathrm{I}_n+\alpha_\gamma\lambda\mathrm{diag}(|z_{1,\mathrm{i}}|_{\lambda-1}))K_1\left|z_2\right|_{p/q-1}z_1^Tz_2
\end{aligned}\tag{A14}$$

Defining the positive definite matrix

$$Q=\begin{bmatrix}Q_{11} & Q_{12}\\ -I_n & O_n\end{bmatrix}\tag{A15}$$

where

$$Q_{11}=2K_1+\alpha_\gamma(\lambda+1)K_1\mathrm{diag}(\left|z_{1,\mathrm{i}}\right|_{\lambda-1})+\alpha_\gamma^2\lambda K_1\mathrm{diag}(\left|z_{1,\mathrm{i}}\right|_{2\lambda-2})\,Q_{12}=\frac{1}{\beta}(\mathrm{I}_n+\alpha_\gamma\lambda\mathrm{diag}(|z_{1,\mathrm{i}}|_{\lambda-1}))K_1\cdot\mathrm{diag}(|z_2|^{p/q-1})$$

then yields

$$z_1^T(-K_1z_1+z_2)-\left(\mathrm{I}_n+\alpha_\gamma\lambda|z_1|^{\lambda-1}\right)K_1z_1^T\boldsymbol{s}=-\begin{bmatrix}z_1^T & z_2^T\end{bmatrix}Q\begin{bmatrix}z_1\\ z_2\end{bmatrix}\tag{A16}$$

and

$$\begin{aligned}
&\dot{V}_2=z_1^T\dot{z}_1+s^T\dot{s}+\frac{1}{\gamma_d}\tilde{d}^T\dot{\tilde{d}}\\
&=-\begin{bmatrix}z_1^T & z_2^T\end{bmatrix}Q\begin{bmatrix}z_1\\ z_2\end{bmatrix}+\boldsymbol{s}^Tz_2+\frac{1}{\gamma_d}\tilde{\boldsymbol{d}}^T\dot{\tilde{\boldsymbol{d}}}+\boldsymbol{s}^T\frac{1}{\beta}\cdot\frac{p}{q}|z_2|^{(p/q-1)}\left(f_2+g_2\boldsymbol{U}_{BTSMC}+K_1\dot{\boldsymbol{z}}_1-\ddot{\boldsymbol{x}}_{1d}+\boldsymbol{d}\right)\\
&=-\begin{bmatrix}z_1^T & z_2^T\end{bmatrix}Q\begin{bmatrix}z_1\\ z_2\end{bmatrix}+\boldsymbol{s}^Tz_2+\frac{1}{\gamma_d}\tilde{\boldsymbol{d}}^T\dot{\tilde{\boldsymbol{d}}}+\boldsymbol{s}^T\frac{1}{\beta}\cdot\frac{p}{q}|z_2|^{(p/q-1)}\\
&\cdot\left(-\beta\cdot\frac{q}{p}z_2{}^{(2-p/q)}-\beta\cdot\frac{q}{p}|z_2|^{(1-p/q)}\left(h_s\boldsymbol{s}+\varsigma\,\mathrm{sgn}(\boldsymbol{s})\right)+(\boldsymbol{d}-\hat{\boldsymbol{d}})\right)\\
&=-\begin{bmatrix}z_1^T & z_2^T\end{bmatrix}Q\begin{bmatrix}z_1\\ z_2\end{bmatrix}+\boldsymbol{s}^Tz_2-\boldsymbol{s}^Tz_2-\boldsymbol{s}^T\left(h_s\boldsymbol{s}+\varsigma\,\mathrm{sgn}(\boldsymbol{s})\right)-\boldsymbol{s}^T\frac{1}{\beta}\cdot\frac{p}{q}|z_2|^{(p/q-1)}\tilde{\boldsymbol{d}}+\frac{1}{\gamma_d}\tilde{\boldsymbol{d}}^T\dot{\hat{\boldsymbol{d}}}\,.
\end{aligned}\tag{A17}$$

where h_s and ς are sliding-mode parameters. The sliding-mode term in the backstepping design improves system adaptiveness to model uncertainties, even in the presence of disturbances.

Substituting $s^T\tilde{d}=\tilde{d}^Ts$ into (A17) yields

$$\begin{aligned}
\dot{V}_2&=-\begin{bmatrix}z_1^T & z_2^T\end{bmatrix}Q\begin{bmatrix}z_1\\ z_2\end{bmatrix}-h_s\boldsymbol{s}^T\boldsymbol{s}-\varsigma|\boldsymbol{s}|-\tfrac{1}{\beta}\cdot\tfrac{p}{q}|z_2|^{(p/q-1)}\tilde{\boldsymbol{d}}+\tilde{\boldsymbol{d}}^T\left(\tfrac{1}{\gamma_d}\dot{\hat{\boldsymbol{d}}}\right)\\
&=-\begin{bmatrix}z_1^T & z_2^T\end{bmatrix}Q\begin{bmatrix}z_1\\ z_2\end{bmatrix}-h_s\boldsymbol{s}^2-\varsigma|\boldsymbol{s}|+\tilde{\boldsymbol{d}}^T\left(\tfrac{1}{\gamma_d}\dot{\hat{\boldsymbol{d}}}-\tfrac{1}{\beta}\cdot\tfrac{p}{q}|z_2|^{(p/q-1)}\boldsymbol{s}\right)
\end{aligned}\tag{A18}$$

The update law is chosen as follows:

$$\dot{\hat{\boldsymbol{d}}}=\gamma_d\frac{1}{\beta}\cdot\frac{p}{q}\left|z_2\right|_{(p/q-1)}\boldsymbol{s},\tag{A19}$$

and if $h > 0, \varsigma > 0$, then

$$\dot{V} = -\begin{bmatrix} z_1^T & z_2^T \end{bmatrix} Q \begin{bmatrix} z_1 \\ z_2 \end{bmatrix} - h_s s^2 - \varsigma |s| < 0. \tag{A20}$$

Therefore, the robust stability of the closed-loop system can be guaranteed by using the DO-BTSMC controller according to Lyapunov theory.

Appendix B. Expression for the *T* Functions

Unsteady aerodynamic load expressions in two-dimensional incompressible flow by Theodorsen are as follows:

$$\begin{aligned}
&T_1 = \tfrac{1}{3}(2+c^2)\sqrt{1-c^2} + c\cos^{-1}c, \\
&T_3 = -\tfrac{1}{8}(1-c^2)(4+5c^2) + \tfrac{1}{4}c(7+2c^2)\sqrt{1-c^2}\cos^{-1}c - (\tfrac{1}{8}+c^2)(\cos^{-1}c)^2, \\
&T_4 = c\sqrt{1-c^2} - \cos^{-1}c, T_5 = -(1-c^2) - (\cos^{-1}c)^2 + 2c\sqrt{(1-c^2)}\cos^{-1}c \\
&T_7 = -\tfrac{1}{8}(7+2c^2)\sqrt{1-c^2} - (\tfrac{1}{8}+c^2)\cos^{-1}c, \\
&T_8 = -\tfrac{1}{3}(1+2c^2)\sqrt{1-c^2} + c\cos^{-1}c, \\
&T_9 = \tfrac{1}{2}\left(\tfrac{1}{3}(1-c^2)^{3/2} + aT_4\right), T_{10} = \sqrt{1-c^2} + \cos^{-1}c, \\
&T_{11} = (2-c)\sqrt{1-c^2} + (1-2c)\cos^{-1}c, T_{12} = (2+c)\sqrt{(1-c^2)} - (1+2c)\cos^{-1}c \\
&T_{13} = -0.5(T_7 + (c-a)T_1), T_{14} = \tfrac{1}{16} + \tfrac{ac}{2}, T_{15} = T_4 + T_{10}, T_{16} = T_1 - T_8 - (c-a)T_4 + 0.5T_{11}, \\
&T_{17} = -2T_9 - T_1 + (a-0.5)T_4, T_{18} = T_5 - T_4T_{10}, T_{19} = -0.5T_4T_{11}
\end{aligned} \tag{A21}$$

References

1. Dowell, E.H. *A Modern Course in Aeroelasticity*, 4th ed.; Kluwer Academic Publisher: Norwell, MA, USA, 2005.
2. Gordon, J.T.; Meyer, E.E.; Minogue, R.L. Nonlinear stability analysis of control surface flutter with freeplay effects. *J. Aircr.* **2008**, *45*, 1904–1916. [CrossRef]
3. Mukhopadhyay, V. Historical perspective on analysis and control of aeroelastic responses. *J. Guid. Control Dyn.* **2003**, *26*, 673–684. [CrossRef]
4. Chai, Y.; Gao, W.; Ankay, B.; Li, F.; Zhang, C. Aeroelastic analysis and flutter control of wings and panels: A review. *Int. J. Mech. Syst. Dyn.* **2021**, *1*, 5–34. [CrossRef]
5. Ouyang, Y.; Gu, Y.; Kou, X.; Yang, Z. Active flutter suppression of wing with morphing flap. *Aerosp. Sci. Technol.* **2021**, *110*, 106457. [CrossRef]
6. Na, S.; Song, J.S.; Choo, J.H.; Qin, Z.M. Dynamic aeroelastic response and active control of composite thin-walled beam structures in compressible flow. *J. Sound Vib.* **2011**, *330*, 4998–5013. [CrossRef]
7. O'Neil, T.; Strganac, T.W. Aeroelastic response of a rigid wing supported by nonlinear springs. *J. Aircr.* **1998**, *35*, 673–684. [CrossRef]
8. Lee, H.K.; Jiang, L.Y.; Wong, Y.S. Flutter of an airfoil with a cubic nonlinear restoring force. *J. Fluids Struct.* **1999**, *13*, 75–101. [CrossRef]
9. Singh, S.N.; Wang, L. Output feedback form and adaptive stabilization of a nonlinear aeroelastic system. *J. Guid. Control Dyn.* **2002**, *25*, 725–732. [CrossRef]
10. Lin, C.M.; Chin, W.L. Adaptive decouple fuzzy sliding mode control of a nonlinear aeroelastic system. *J. Guid. Control Dyn.* **2006**, *29*, 206–209. [CrossRef]
11. Chen, C.L.; Chang, C.W.; Yau, H.T. Terminal sliding mode control for aeroelastic systems. *Nonlinear Dyn.* **2012**, *70*, 2015–2026. [CrossRef]
12. Bouma, A.; Basconcellos, R.; Abdelkefi, A. Nonlinear aeroelastic modeling and comparative studies of three degrees of freedom wing-based systems. *Int. J. Non-Linear Mech.* **2023**, *149*, 104326. [CrossRef]
13. Vishal, S.; Ashwad, R.; Chandan, B.; Venkatramani, J. Routes to Synchronization in a pitch–plunge aeroelastic system with coupled structural and aerodynamic nonlinearities. *Int. J. Non-Linear Mech.* **2021**, *135*, 103766. [CrossRef]
14. Livne, E. Active Flutter suppression state of the art and technology maturation needs. *J. Aircr.* **2018**, *55*, 410–450. [CrossRef]
15. Zou, Q.T.; Huang, R.; Hu, H.Y. Body-freedom flutter suppression for a flexible flying-wing drone via time-delayed control. *J. Guid. Control Dyn.* **2022**, *45*, 28–38. [CrossRef]
16. Trapani, M.; Guo, S. Design and analysis of a rudderless aeroelastic fin. *Proc. IMechE Part G J. Aerosp. Eng.* **2009**, *223*, 701–710. [CrossRef]
17. Zhang, K.; Behal, A. Continuous robust control for aeroelastic vibration control of a 2-D airfoil under unsteady flow. *J. Vib. Control* **2016**, *22*, 2841–2860. [CrossRef]
18. Lee, K.W.; Singh, S.N. L_1 Adaptive control of an aeroelastic System with unsteady aerodynamics and gust Load. *J. Vib. Control* **2016**, *24*, 303–322. [CrossRef]

19. Platanitis, G.; Strganac, T.W. Control of a nonlinear wing section using leading- and trailing-edge surfaces. *J. Guid. Control Dyn.* **2004**, *27*, 52–58. [CrossRef]
20. Prime, Z.D. Robust Scheduling Control of Aeroelasticity. Ph.D. Thesis, University of Adelaide, Adelaide, Australia, 2010.
21. Li, D.C.; Guo, S.J.; Xiang, J.W. Aeroelastic dynamic response and control of an airfoil section with control surface nonlinearities. *J. Sound Vib.* **2010**, *329*, 4756–4771. [CrossRef]
22. Tang, L.D.; Chen, Z.; Tian, F.; Hu, E. A neural network approach for improving airfoil active flutter suppression under control input constraints. *J. Vib. Control* **2021**, *27*, 451–467. [CrossRef]
23. Gao, M.Z.; Cai, G.P.; Nan, Y. Finite-time fault-tolerant control for flutter of wing. *Control Eng. Pract.* **2016**, *51*, 26–47.
24. Chen, Z.; Shi, Z.W.; Chen, S.N.; Tong, S.X. Active flutter suppression for a flexible wing model with trailing-edge circulation control via reinforcement learning. *AIP Adv.* **2023**, *13*, 015317. [CrossRef]
25. Pettit, C.L. Uncertainty quantification in aeroelasticity: Recent results and research challenges. *J. Aircr.* **2004**, *41*, 1217–1229. [CrossRef]
26. Hao, Y.; Ma, C.; Hu, Y.D. Nonlinear stochastic flutter analysis of a three-degree-of-freedom wing in a two-dimensional flow field under stochastic perturbations. *Aerosp. Sci. Technol.* **2023**, *138*, 108323. [CrossRef]
27. Lee, K.W.; Singh, S.N. Robust higher-order super-twisting control of aeroelastic system with unsteady aerodynamics. In Proceedings of the 2018 AIAA Guidance, Navigation, and Control Conference, AIAA SciTech Forum, Kissimmee, FL, USA, 8–12 January 2018; pp. 2018–2341.
28. Prabhu, L.; Srinivas, J. Robust control of a three degrees of freedom aeroelastic model using an intelligent observer. In Proceedings of the 2015 International Conference on Robotics, Automation, Control and Embedded Systems (RACE), Chennai, India, 18–20 February 2015; pp. 1–5.
29. Yuan, J.X.; Qi, N.; Qiu, Z.; Wang, F.X. Sliding Mode Observer Controller Design for a Two Dimensional Aeroelastic System with Gust Load. *Asian J. Control* **2019**, *21*, 130–142. [CrossRef]
30. Xu, X.; Wu, W.; Zhang, W. Sliding mode control for a nonlinear aeroelastic system through backstepping. *J. Aerosp. Eng.* **2018**, *31*, 04017080. [CrossRef]
31. Chen, W.H.; Yang, J.; Guo, L.; Li, S. Disturbance-observer-based control and related methods—An overview. *IEEE Trans. Ind. Electron.* **2016**, *63*, 1083–1095. [CrossRef]
32. Liu, S.Q.; Whidborne, J.F. Neural network adaptive backstepping fault tolerant control for unmanned airships with multi-vectored thrusters. *Proc. IMechE Part G J. Aerosp. Eng.* **2021**, *235*, 1507–1520. [CrossRef]
33. Thordorsen, T.; Garrice, I.E. *Nonstatoinary Flow about a Wing Aileron Tab Combination Including Aerodynamic Balance*; 19930091815, NACA Report No. 736; US Government Printing Office: Washington, DC, USA, 1942; pp. 129–138.
34. Edwards, J.W. Unsteady Aerodynamic Modeling and Active Aeroelastic Control. Ph.D. Thesis, Stanford University, Stanford, CA, USA, 1977.
35. Theodorsen, T. *General Theory of Aerodynamic Instability and Mechanism of Flutter*; NACA Report No. 496; US Government Printing Office: Washington, DC, USA, 1935; pp. 291–311.
36. Marzocca, P.; Librescu, L.; Chiocchia, G. Aeroelastic response of 2-D lifting surfaces to gust and arbitrary explosive loading signatures. *Int. J. Impact Eng.* **2001**, *25*, 41–65. [CrossRef]
37. Chen, W.H.; Ballance, D.J.; Gawthrop, P.J.; O'Reilly, J. A nonlinear disturbance roobserver for robotic manipulators. *IEEE Trans. Ind. Electron.* **2000**, *47*, 932–938. [CrossRef]
38. Prime, Z.; Cazzolato, B.; Doolan, C.; Strganac, T. Linear-parameter-varying control of an improved three-degree-of-freedom aeroelastic model. *J. Guid. Control Dyn.* **2010**, *33*, 615–618. [CrossRef]
39. Hassig, H. An approximate true damping solution of the flutter equation by determinant iteration. *J. Aircr.* **1971**, *8*, 885–889. [CrossRef]
40. Liu, S.Q.; Whidborne, J.F.; He, L. Backstepping sliding-mode control of stratospheric airships using disturbance-observer. *Adv. Space Res.* **2021**, *67*, 1174–1187. [CrossRef]
41. Van, M.; Mavrovouniotis, M.; Ge, S.S. An adaptive backstepping nonsingular fast terminal sliding mode control for robust fault tolerant control of robot manipulators. *IEEE Trans. Syst. Man Cybern. Part B Cybern.* **2019**, *49*, 1448–1458. [CrossRef]

Disclaimer/Publisher's Note: The statements, opinions and data contained in all publications are solely those of the individual author(s) and contributor(s) and not of MDPI and/or the editor(s). MDPI and/or the editor(s) disclaim responsibility for any injury to people or property resulting from any ideas, methods, instructions or products referred to in the content.

https://dspace.org/

Disturbance observer-based backstepping terminal sliding mode aeroelastic control of airfoils

Liu, Shiqian; Yang, Congjie; Zhang, Qian; Whidborne, James F.

2024-11-01
MDPI
https://doi.org/10.3390/aerospace11110882
Liu S, Yang C, Zhang Q, Whidborne JF (2024) Disturbance observer-based backstepping terminal sliding mode aeroelastic control of airfoils. Aerospace, Volume 11, Issue 11, November 2024, Article number 882

Downloaded from a DSpace repository. https://dspace.org/